Numeric implementation of wave-equation migration velocity analysis operators

Paul Sava[1] and Ioan Vlad[2]
[1] *Center for Wave Phenomena, Colorado School of Mines*
[2] *StatoilHydro, Trondheim, Norway*

ABSTRACT

Wave-equation migration velocity analysis (MVA) is a technique similar to wave-equation tomography because it is designed to update velocity models using information derived from full seismic wavefields. On the other hand, wave-equation MVA is similar to conventional, traveltime-based MVA because it derives the information used for model updates from properties of migrated images, e.g. focusing and moveout. The main motivation for using wave-equation MVA is derived from its consistency with the corresponding wave-equation migration, which makes this technique robust and capable of handling multipathing characterizing media with large and sharp velocity contrasts. The wave-equation MVA operators are constructed using linearizations of conventional wavefield extrapolation operators, assuming small perturbations relative to the background velocity model. Similarly to typical wavefield extrapolation operators, the wave-equation MVA operators can be implemented in the mixed space-wavenumber domain using approximations of different orders of accuracy.
As for wave-equation migration, wave-equation MVA can be formulated in different imaging frameworks, depending on the type of data used and image optimization criteria. Examples of imaging frameworks correspond to zero-offset migration (designed for imaging based on focusing properties of the image), survey-sinking migration (designed for imaging based on moveout analysis using narrow-azimuth data) and shot-record migration (also designed for imaging based on moveout analysis, but using wide-azimuth data).
The wave-equation MVA operators formulated for the various imaging frameworks are similar because they share common elements derived from linearizations of the single square-root equation. Such operators represent the core of iterative velocity estimation based on diffraction focusing or semblance analysis, and their applicability in practice requires efficient and accurate implementation. This tutorial concentrates strictly on the numeric implementation of those operators and not on their use for iterative migration velocity analysis.

Key words: wave-equation, migration, velocity analysis

1 INTRODUCTION

Accurate wave-equation depth imaging requires accurate knowledge of a velocity model. The velocity model is used in the process of wavefield reconstruction, irrespective of the method used to solve the acoustic wave-equation, e.g. by integral methods (Kirchhoff migration), or by differential/spectral methods (migration by wavefield extrapolation and reverse-time migration).

Generally-speaking, there are two possible strategies for velocity estimation from surface seismic data in the context of wavefield depth migration. The two strategies differ by the domain in which the information used to update the velocity model is collected. The first strategy is formulated in the *data space*, prior to migration, and it involves matching of recorded

and simulated data using an approximate (background) velocity model. Techniques in this category are known by the name of tomography (or inversion). The second strategy is formulated in the *image space*, after migration, and it involves measuring and correcting image features that indicate model inaccuracies. Techniques in this category are known as migration velocity analysis (MVA), since they involve migrated images and not the recorded data directly.

Tomography and migration velocity analysis can be implemented in various ways that can be classified based on the carrier of information from the data or image to the velocity model. Thus, we can distinguish between *ray-based* methods and *wave-based* methods. This terminology is applicable to both tomography and migration velocity analysis. For ray-based methods, the carrier of information are wide-band rays traced using a background velocity model from picked events in the data (or image). Methods in this category are known as *traveltime tomography* (Bishop *et al.*, 1985) and *traveltime MVA*, sometimes described as image-space traveltime tomography (Stork, 1992; Al-Yahya, 1987; Fowler, 1988; Etgen, 1990; Chavent & Jacewitz, 1995; Clement *et al.*, 2001; Chauris *et al.*, 2002a,b; Billette *et al.*, 2003; Lambare *et al.*, 2004; Clapp *et al.*, 2004). For wave-based methods, the carrier of information are band-limited wavefields constructed using a background velocity model. Methods in this category are known as *wave-equation tomography* (Gauthier *et al.*, 1986; Tarantola, 1987; Mora, 1989; Woodward, 1992; Pratt, 1999, 2004), and *wave-equation MVA* (Biondi & Sava, 1999; Sava & Biondi, 2004a,b; Shen *et al.*, 2005; Albertin *et al.*, 2006b; Maharramov & Albertin, 2007). This paper concentrates on methods from the latter category.

The volume of information used for model updates using wave-based methods is at least one order of magnitude larger than the volume of information used for ray-based methods. Thus, a fundamental question we should ask is what is gained by using wave-based methods over ray-based methods. First, modern imaging applications using wave-based methods (downward continuation or reverse-time extrapolation) require consistent velocity estimation methods which interact with model in the same frequency band as the migration methods. Second, wave-based methods are robust (i.e. stable) for models with large and sharp velocity variations (e.g. salt). Third, wave-based methods describe naturally all propagation paths, thus they can easily handle multi-pathing characterizing wave propagation in media with large velocity variations.

Wave-equation tomography and wave-equation MVA have both similarities and differences. Wave-equation tomography uses the advantage that the residual used for velocity updating is obtained by a direct comparison between recorded and measured data. In contrast, wave-equation MVA uses the property that the residual used for velocity updating is obtained by a comparison between a reference image and an improved version of it. On the other hand, wave-equation tomography has the disadvantage that the kinematics of events in the data domain are more complex than in the image domain. In addition, the dimensionality of the space in which to evaluate the misfit between recorded and simulated data is higher too, potentially making a comparison more complex. Also, wave-equation MVA optimizes directly the desired end product, i.e. the migrated image, which potentially makes this technique more "interpretive" and less of a computational "black-box".

One important component of MVA methods is what type of measurement on migrated images is used to evaluate its deficiencies. Although strictly related to one-another, we can describe two kinds of information available to quantify image quality. First is *focusing analysis*, which evaluates whether point-like events, e.g. fault truncations, are focused in migrated images at their correct position. Image enhancement for wave-equation MVA can be formulated purely based on this type of information, which makes the techniques fast since it only operates with zero-offset data (Sava *et al.*, 2005). Second is *moveout analysis*, which is the case for all conventional MVA techniques, whether using rays or waves. In this case, we can formulate wave-equation MVA based on analysis of moveout of common-image gathers using velocity scans (Biondi & Sava, 1999; Sava & Biondi, 2004a,b) or based on analysis of differential semblance of nearby traces in similar common-image gathers (Shen *et al.*, 2005).

Moveout analysis requires construction of common-image gathers (CIGs) characterizing the dependence of reflectivity function of various parameters used to parametrize multiple experiments used for imaging. There are two main alternatives for common-image gather construction. First, we can construct *offset-domain* CIGs (Yilmaz & Chambers, 1984), when reflectivity depends on source-receiver offset on the acquisition surface, which is a data parameter. Second, we can construct *angle-domain* CIGs (de Bruin *et al.*, 1990; Prucha *et al.*, 1999; Mosher & Foster, 2000; Rickett & Sava, 2002; Xie & Wu, 2002; Sava & Fomel, 2003; Soubaras, 2003; Fomel, 2004; Biondi & Symes, 2004), when reflectivity depends on the angles of incidence at the reflection point, which is an image parameter. For wave-equation migration, offset-domain CIGs are not a practical solution, since the information from multiple offsets (or multiple seismic experiments) mixes in the process of migration. Furthermore, angle-domain CIGs suffer from fewer artifacts than offset-domain CIGs, due to the fact that reflectivity parametrization for angle-gathers occurs after wavefield reconstruction in the subsurface, as oppose to offset-gathers when reflectivity parametrization is related to data parameters (Stolk & Symes, 2004).

Both wave-equation tomography and wave-equation MVA methods are based on a fundamental "small perturbation" assumption, which requires a reasonably-good starting model. This requirement represents a drawback which is responsible for the main difficulty of methods in both categories. For wave-equation tomography or inversion, we can update models based on differences between recorded and simulated data. If the starting background model is not accurate enough, we run the risk of subtracting wavefields corresponding to different events. Likewise, for wave-equation MVA, we update the model based on differences between two images, one simulated in the background model and an enhanced version of this image. If the enhanced version of the image goes too far from the reference image, we run the risk of subtracting events

corresponding to different reflectors. This phenomenon is usually referred-to in the literature as "cycle skipping" and various strategies have been designed to ameliorate this problem, e.g. by optimal selection of frequencies used for velocity analysis (Sirgue & Pratt, 2004; Albertin, 2006). However, alternative methods used to evaluate image accuracy, e.g. differential semblance (Symes & Carazzone, 1991; Shen *et al.*, 2003), have the best potential to ameliorate this situation. In this case wave-equation MVA analyzes difference between image traces within common-image gathers which are likely to be similar enough from one-another such as to avoid the cycle-skipping problem. Even in this case, the assumption made is that the nearby traces in a gather are sampled well-enough, i.e. the seismic events differ by only a fraction of the wavelet, which is a function of image sampling and frequency content. In practice, there is no absolute guarantee that nearby events are closely related to one another, although this is more likely to be true for DSO than it is for direct image differencing.

In this paper, we concentrate on the implementation of the wave-equation migration velocity analysis operators for various wave-equation migration configurations. The main objective of the paper is to derive the linearized operators linking perturbations of the slowness model to the corresponding perturbations of the seismic wavefield and image. All our theoretical development is formulated under the single scattering (Born) approximation applied to acoustic waves. We begin by describing the MVA operators corresponding to zero-offset, survey-sinking and shot-record wave-equation migration frameworks. We describe the theoretical background for each operator and emphasize the similarities and differences between the different operators. Throughout the paper, we use pseudo-code to illustrate implementation strategies and data flow for the various wave-equation MVA operators. Finally, we illustrate the wave-equation MVA operators with impulse responses corresponding to simple and complex models. We leave outside the scope of this paper the procedure in which the discussed operators are used for migration velocity analysis.

2 WAVE-EQUATION MIGRATION AND VELOCITY ANALYSIS OPERATORS

The conceptual framework of wave-equation MVA is similar to that of conventional (ray-based) MVA in that the source of information for velocity updating is extracted from features of migrated images. This is in contrast with wave-equation tomography (or inversion), where the source of information is represented by the mismatch between recorded and simulated data. The main difference between wave-equation MVA and ray-based MVA is that the carrier of information from the migrated images to the velocity model is represented by the entire extrapolated wavefield and not by a rayfield constructed from selected points in the image based on an approximate velocity model.

The key element for the wave-equation MVA technique is a definition of an *image perturbation* corresponding to the difference between the image obtained with a known background velocity model and an improved image. Such image perturbations can be constructed using straight differences between images (Biondi & Sava, 1999; Albertin *et al.*, 2006a), or by examining moveout parameters in migrated images (Sava & Biondi, 2004a,b; Shen *et al.*, 2005; Albertin *et al.*, 2006b; Maharramov & Albertin, 2007). Then, using wave-equation MVA operators, the image perturbations can be translated into *slowness perturbations* which update the model. The direct analogy between wave-based MVA and ray-based MVA is the following: wave-based methods use image perturbations and back-propagation using waves, while ray-based methods use traveltime perturbations and back-propagation using rays. Thus, wave-equation MVA benefits from all the characteristics of wave-based imaging techniques, e.g. stability in areas of large velocity variation, while remaining conceptually similar to conventional traveltime-based MVA.

We can formulate wave-equation migration and velocity analysis for different configurations in which we process the recorded data. There are two main classes of wave-equation migration, *survey-sinking migration* and *shot-record migration* (Claerbout, 1985), which differ in the way in which recorded data are processed. Both wave-equation imaging techniques use similar algorithms for downward continuation and, in theory, produce identical images for identical implementation of extrapolation operators and if all data are used for imaging (Berkhout, 1982; Biondi, 2003). The main difference is that shot-record migration is used to process separate seismic experiments (shots) sequentially, while survey-sinking migration is used to process all seismic experiments (shots) simultaneously. The shot-record operators are more computationally expensive but less memory intensive than the survey-sinking operators. A special case of survey-sinking migration assumes the sources and receivers are coincident on the acquisition surface, a technique usually described as the exploding reflector model (Loewenthal *et al.*, 1976) applicable to zero-offset data. All operators described here can be used in models characterized by complex wave propagation (multipathing).

In all situations, wave-equation migration can be formulated as consisting of two main steps. The first step is *wavefield reconstruction* (abbreviated W.R. for the rest of this paper) at all locations in space and using all frequencies from the recorded data as boundary conditions. This step requires numeric solutions to a form of wave equation, typically the one-way acoustic wave equation. The second step is the *imaging condition* (abbreviated I.C. for the rest of this paper), which is used to extract from the reconstructed wavefield(s) the locations where reflectors occur. This step requires numeric implementation of image processing techniques, e.g. cross-correlation, which evaluate properties of the wavefield indicating the presence of reflectors. Needless to say, the two steps are not implemented sequentially in practice, since the size of the wavefield is usually large and cannot be handled efficiently on conventional computers. Instead, wavefield reconstruction and imaging condition are implemented on-the-fly, avoiding expensive data storage and retrieval. Wave-equation MVA requires implementation of an additional procedure which links

image and slowness perturbations. This link is given by a *wavefield scattering* operation (abbreviated W.S. for the rest of this paper) which is derived by linearization from conventional wavefield extrapolation operators.

In the following sections, we describe the migration and velocity analysis operators for the various imaging configurations. We begin with zero-offset imaging under the exploding reflector model, because this is the simplest wave-equation imaging framework and can aid our understanding of both survey-sinking and shot-record migration and velocity analysis frameworks. We then continue with a description of the wave-equation migration velocity analysis operator for multi-offset data using the survey-sinking and shot-record migration configuration. For each configuration, we describe the implementation of the *forward operator* (used to translate model perturbations into image perturbations) and of the *adjoint operator* (used to transform image perturbations into model perturbations). Both forward and adjoint operators are necessary for the implementation of efficient numeric conjugate gradient optimization (Claerbout, 1985). Throughout this paper, we are using the following notations and naming conventions:

- ω: angular frequency
- z: depth coordinate
- $\mathbf{m} = \{m_x, m_y\}$: midpoint coordinates
- $\mathbf{h} = \{h_x, h_y\}$: half-offset coordinates
- $\mathbf{k_m} = \{k_{m_x}, k_{m_y}\}$: midpoint wavenumbers
- $\mathbf{k_h} = \{k_{h_x}, k_{h_y}\}$: half-offset wavenumbers
- $s(\mathbf{m})$: medium slowness
- $s_0(\mathbf{m})$: background slowness
- $u(\mathbf{m})$ or $u(\mathbf{m}, \mathbf{h})$: wavefield at frequency ω and depth z for zero-offset and multiple-offset data, respectively
- $\Delta u(\mathbf{m})$ or $\Delta u(\mathbf{m}, \mathbf{h})$: scattered wavefield at frequency ω and depth z for zero-offset and multiple-offset data, respectively
- $r(\mathbf{m})$ or $r(\mathbf{m}, \mathbf{h})$: image at depth z for zero-offset and multiple-offset data, respectively
- I.C.: imaging condition
- W.R.: wavefield extrapolation
- W.S.: wavefield scattering
- $\mathcal{E}^{\pm}[]$: extrapolation operator (causal for $+$, anticausal for $-$)
- $\mathcal{F}^{\pm}[]$: forward scattering operator (causal for $+$, anticausal for $-$)
- $\mathcal{A}^{\mp}[]$: adjoint scattering operator (causal for $+$, anticausal for $-$)

2. 1 Zero-offset migration and velocity analysis

Wavefield reconstruction for zero-offset migration based on the one-way wave-equation is performed by recursive phase-shift in depth starting with data recorded on the surface as boundary conditions. In this configuration, the imaging condition extracts the image as time $t = 0$ from the reconstructed wavefield at every location in space. Thus, the surface data need to be extrapolated backward in time which is achieved by selecting the appropriate sign of the phase-shift operation (which depends on the sign convention for temporal Fourier transforms):

$$u_{z+\Delta z}(\mathbf{m}) = e^{-ik_z \Delta z} u_z(\mathbf{m}) \ . \tag{1}$$

In equation 1, $u_z(\mathbf{m})$ represents the acoustic wavefield at depth z for a given frequency ω at all positions in space $\mathbf{m}$, and $u_{z+\Delta z}(\mathbf{m})$ represents the same wavefield extrapolated to depth $z + \Delta z$. The phase shift operation uses the depth wavenumber k_z which is defined by the single square-root (SSR) equation

$$k_z = \sqrt{[2\omega s(\mathbf{m})]^2 - |\mathbf{k_m}|^2} \ , \tag{2}$$

where $s(\mathbf{m})$ represents the spatially-variable slowness at depth level z. Equations 1-2 describe wavefield extrapolation using a pseudo-differential operator, which justifies our use of laterally-varying slowness $s(\mathbf{m})$. As indicated earlier, the image is obtained from this extrapolated wavefield by selection of time $t = 0$, which is typically implemented as summation of the extrapolated wavefield over frequencies:

$$r_z(\mathbf{m}) = \sum_{\omega} u_z(\mathbf{m}, \omega) \ . \tag{3}$$

Phase-shift extrapolation using wavenumbers computed using equations 1 and 2 is not feasible in media with lateral variation. Instead, implementation of such operators is done using approximations implemented in a mixed space-wavenumber domain (Stoffa *et al.*, 1990; Ristow & Ruhl, 1994; Huang *et al.*, 1999). A brief summary the mixed-domain implementation of the split-step Fourier (SSF) operator is presented in Appendix A.

For velocity analysis, we assume that we can separate the *total slowness* $s(\mathbf{m})$ into a known background component $s_0(\mathbf{m})$ and an unknown component $\Delta s(\mathbf{m})$. With this convention, we can linearize the depth wavenumber k_z relative to the background slowness s_0 using a truncated Taylor series expansion

$$k_z \approx k_{z0} + \left. \frac{dk_z}{ds} \right|_{s_0} \Delta s(\mathbf{m}) \ , \tag{4}$$

where the depth wavenumber in the background medium characterized by slowness $s_0(\mathbf{m})$ is

$$k_{z0} = \sqrt{[2\omega s_0(\mathbf{m})]^2 - |\mathbf{k_m}|^2} \ . \tag{5}$$

Here, $s_0(\mathbf{m})$ represents the spatially-variable *background slowness* at depth level z. Using the wavenumber linearization from equation 4, we can reconstruct the acoustic wavefields in the background model using a phase-shift operation

$$u_{z+\Delta z}(\mathbf{m}) = e^{-ik_{z0} \Delta z} u_z(\mathbf{m}) \ . \tag{6}$$

We can represent wavefield extrapolation using a generic solution to the one-way wave-equation using the notation $u_{z+\Delta z}(\mathbf{m}) = \mathcal{E}^{-}_{ZOM}[2s_{0z}(\mathbf{m}), u_z(\mathbf{m})]$. This notation indicates that the wavefield $u_{z+\Delta z}(\mathbf{m})$ is reconstructed from the wavefield $u_z(\mathbf{m})$ using the background slowness $s_0(\mathbf{m})$. This operation is repeated independently for all frequencies ω.

A typical implementation of zero-offset wave-equation migration uses the following algorithm:

ZERO-OFFSET MIGRATION ALGORITHM

$\omega = \omega_{min} \dots \omega_{max}\{$
  read $u(\mathbf{m})$
  $z = z_{min} \dots z_{max}\{$
    write $u(\mathbf{m})$
    read $r(\mathbf{m})$
    $r(\mathbf{m}) += u(\mathbf{m})$
    write $r(\mathbf{m})$
    $u(\mathbf{m}) = \mathcal{E}^{-}_{ZOM}[2s_0(\mathbf{m}), u(\mathbf{m})]$
  $\}$
$\}$

A seismic image is produced using migration by wavefield extrapolation as follows: for each frequency, read data at all spatial locations $\mathbf{m}$; then, for each depth, sum the wavefield into the image at that depth level (i.e. apply the imaging condition) and then reconstruct the wavefield to the next depth level (i.e. perform wavefield extrapolation). The "-" sign in this algorithm indicates that extrapolation is anti-causal (backward in time), and the factor "2" indicates that we are imaging data recorded in two-way traveltime with an algorithm designed under the exploding reflector model. Wavefield extrapolation is usually implemented in a mixed domain (space-wavenumber), as briefly summarized in Appendix A.

The wavefield perturbation $\Delta u(\mathbf{m})$ caused at depth $z + \Delta z$ by a slowness perturbation $\Delta s(\mathbf{m})$ at depth z is obtained by subtraction of the wavefields extrapolated from z to $z + \Delta z$ in the true and background models:

$$\begin{aligned} \Delta u_{z+\Delta z}(\mathbf{m}) & \qquad (7) \\ &= e^{-ik_z \Delta z} u_z(\mathbf{m}) - e^{-ik_{z0} \Delta z} u_z(\mathbf{m}) \\ &= e^{-ik_{z0}\Delta z}\left[e^{-i\frac{dk_z}{ds}\big|_{s_0}\Delta s(\mathbf{m})\Delta z} - 1\right] u_z(\mathbf{m}) \qquad (8) \end{aligned}$$

Here, $\Delta u(\mathbf{m})$ and $u(\mathbf{m})$ correspond to a given depth level z and frequency ω. A similar relation can be applied at all depths and all frequencies.

Equation 8 establishes a non-linear relation between the wavefield perturbation $\Delta u(\mathbf{m})$ and the slowness perturbation $\Delta s(\mathbf{m})$. Given the complexity and cost of numeric optimization based on non-linear relations between model and wavefield parameters, it is desirable to simplify this relation to a linear relation between model and data parameters. Assuming small slowness perturbations, i.e. small phase perturbations, the exponential function $e^{\pm i\frac{dk_z}{ds}\big|_{s_0}\Delta s(\mathbf{m})\Delta z}$ can be linearized using the approximation $e^{i\phi} \approx 1 + i\phi$ which is valid for small values of the phase ϕ. Therefore the wavefield perturbation $\Delta u(\mathbf{m})$ at depth z can be written as

$$\begin{aligned} \Delta u(\mathbf{m}) &\approx -i\left.\frac{dk_z}{ds}\right|_{s_0} \Delta z\, u(\mathbf{m})\, \Delta s(\mathbf{m}) \\ &\approx -i\Delta z \frac{2\omega u(\mathbf{m})\, \Delta s(\mathbf{m})}{\sqrt{1 - \left[\frac{|\mathbf{k_m}|}{2\omega s_0(\mathbf{m})}\right]^2}} \,. \qquad (9) \end{aligned}$$

Equation 9 defines the zero-offset forward scattering operator $\mathcal{F}^{-}_{ZOM}[u(\mathbf{m}), 2s_0(\mathbf{m}), \Delta s(\mathbf{m})]$, producing the scattered wavefield $\Delta u(\mathbf{m})$ from the slowness perturbation $\Delta s(\mathbf{m})$, based on the background slowness $s_0(\mathbf{m})$ and background wavefield $u(\mathbf{m})$ at a given frequency ω. The image perturbation at depth z is obtained from the scattered wavefield using the time $t = 0$ imaging condition, similar to the procedure used for imaging in the background medium:

$$\Delta r(\mathbf{m}) = \sum_{\omega} \Delta u(\mathbf{m}, \omega) \,. \qquad (10)$$

Given an image perturbation $\Delta r(\mathbf{m})$, we can construct the scattered wavefield by the adjoint of the imaging condition

$$\Delta u(\mathbf{m}, \omega) = \Delta r(\mathbf{m}) \,, \qquad (11)$$

for every frequency ω. Then, the slowness perturbation at depth z and frequency ω caused by a wavefield perturbation at depth z under the influence of the background wavefield at the same depth z can be written as

$$\begin{aligned} \Delta s(\mathbf{m}) &\approx +i\left.\frac{dk_z}{ds}\right|_{s_0} \Delta z\, \overline{u(\mathbf{m})} \Delta u(\mathbf{m}) \\ &\approx +i\Delta z \frac{2\omega \overline{u(\mathbf{m})} \Delta u(\mathbf{m})}{\sqrt{1 - \left[\frac{|\mathbf{k_m}|}{2\omega s(\mathbf{m})}\right]^2}} \,. \qquad (12) \end{aligned}$$

Equation 12 defines the adjoint scattering operator $\mathcal{A}^{+}_{ZOM}[u(\mathbf{m}), 2s_0(\mathbf{m}), \Delta u(\mathbf{m})]$, producing the slowness perturbation $\Delta s(\mathbf{m})$ from the scattered wavefield $\Delta u(\mathbf{m})$, based on the background slowness $s_0(\mathbf{m})$ and background wavefield $u(\mathbf{m})$. A typical implementation of zero-offset forward and adjoint scattering uses the following algorithms:

ZERO-OFFSET FORWARD SCATTERING ALGORITHM

$\omega = \omega_{min} \dots \omega_{max}\{$
  initialize $\Delta u(\mathbf{m}) = 0$
  $z = z_{min} \dots z_{max}\{$
    read $u(\mathbf{m})$
    read $\Delta s(\mathbf{m})$
    $\Delta u(\mathbf{m}) += \mathcal{F}^{-}_{ZOM}[u(\mathbf{m}), 2s_0(\mathbf{m}), \Delta s(\mathbf{m})]$
    read $\Delta r(\mathbf{m})$
    $\Delta r(\mathbf{m}) += \Delta u(\mathbf{m})$
    write $\Delta r(\mathbf{m})$
    $\Delta u(\mathbf{m}) = \mathcal{E}^{-}_{ZOM}[2s_0(\mathbf{m}), \Delta u(\mathbf{m})]$
  $\}$
$\}$

ZERO-OFFSET ADJOINT SCATTERING ALGORITHM

$\omega = \omega_{min} \dots \omega_{max}\{$
  initialize $\Delta u(\mathbf{m}) = 0$
  $z = z_{max} \dots z_{min}\{$
    read $u(\mathbf{m})$
    $\Delta u(\mathbf{m}) = \mathcal{E}^{+}_{ZOM}[2s_0(\mathbf{m}), \Delta u(\mathbf{m})]$
    read $\Delta r(\mathbf{m})$

$\Delta u\,(\mathbf{m}) += \Delta r\,(\mathbf{m})$
read $\Delta s\,(\mathbf{m})$
$\Delta s\,(\mathbf{m}) += \mathcal{A}^{+}_{ZOM}\left[u\,(\mathbf{m}),2s_0\,(\mathbf{m}),\Delta u\,(\mathbf{m})\right]$
write $\Delta s\,(\mathbf{m})$
}
}

The forward zero-offset wave-equation MVA operator follows a similar pattern to the implementation of the downward continuation operator: for each frequency and for each depth, read the slowness perturbation Δs at all spatial locations $\mathbf{m}$, then apply the scattering operator (W.S.) given equation 12 to the slowness perturbation and accumulate the scattered wavefield for downward continuation; then, apply the imaging condition (I.C.) producing the image perturbation Δr at depth z and then reconstruct the scattered wavefield backward in time using the wavefield extrapolation operator (W.R.) to the next depth level. The adjoint zero-offset wave-equation MVA operator also follows a similar pattern to the implementation of the downward continuation operator: for each frequency and for each depth, reconstruct the scattered wavefield forward in time using the wavefield extrapolation operator (W.R.) to the next depth level, then apply the adjoint of the imaging condition (I.C.) by adding the image to the scattered wavefield and then apply the adjoint wavefield scattering operator (W.S.) to obtain the slowness perturbation Δs. Both forward and adjoint scattering algorithms require the background wavefield, u, to be precomputed at all depth levels, although more efficient implementations using optimal checkpointing are possible (**?**). Scattering and wavefield extrapolation are implemented in the mixed space-wavenumber domain, as briefly explained in Appendix A.

2. 2 Survey-sinking migration and velocity analysis

Wavefield reconstruction for multi-offset migration based on the one-way wave-equation under the survey-sinking framework (Claerbout, 1985) is implemented similarly to the zero-offset case by recursive phase-shift of prestack wavefields

$$u_{z+\Delta z}\,(\mathbf{m},\mathbf{h}) = e^{-ik_z\Delta z}u_z\,(\mathbf{m},\mathbf{h})\ , \tag{13}$$

followed by extraction of the image at time $t=0$. Here, $\mathbf{m}$ and $\mathbf{h}$ stand for midpoint and half-offset coordinates, respectively, defined according to the relations

$$\mathbf{m} = \frac{\mathbf{r}+\mathbf{s}}{2} \tag{14}$$

$$\mathbf{h} = \frac{\mathbf{r}-\mathbf{s}}{2}\ , \tag{15}$$

where $\mathbf{s}$ and $\mathbf{r}$ are coordinates of sources and receivers on the acquisition surface. In equation 13, $u_z\,(\mathbf{m},\mathbf{h})$ represents the acoustic wavefield for a given frequency ω at all midpoint positions $\mathbf{m}$ and half-offsets $\mathbf{h}$ at depth z, and $u_{z+\Delta z}\,(\mathbf{m},\mathbf{h})$ represents the same wavefield extrapolated to depth $z+\Delta z$. The phase shift operation uses the depth wavenumber k_z which is defined by the double square-root (DSR) equation

$$\begin{aligned} k_z &= \sqrt{\left[\omega s\,(\mathbf{m}-\mathbf{h})\right]^2 - \left|\frac{\mathbf{k_m}-\mathbf{k_h}}{2}\right|^2} \\ &+ \sqrt{\left[\omega s\,(\mathbf{m}+\mathbf{h})\right]^2 - \left|\frac{\mathbf{k_m}+\mathbf{k_h}}{2}\right|^2}\ . \end{aligned} \tag{16}$$

The image is obtained from this extrapolated wavefield by selection of time $t=0$, which is usually implemented as summation over frequencies:

$$r_z\,(\mathbf{m},\mathbf{h}) = \sum_{\omega} u_z\,(\mathbf{m},\mathbf{h},\omega)\ . \tag{17}$$

Similarly to the derivation done in the zero-offset case, we can assume the separation of the extrapolation slowness $s\,(\mathbf{m})$ into a background component $s_0\,(\mathbf{m})$ and an unknown perturbation component $\Delta s\,(\mathbf{m})$. Then we can construct a wavefield perturbation $\Delta u\,(\mathbf{m},\mathbf{h})$ at depth z and frequency ω related linearly to the slowness perturbation $\Delta s\,(\mathbf{m})$. Linearizing the depth wavenumber given by the DSR equation 16 relative to the background slowness $s_0\,(\mathbf{m})$, we obtain

$$k_z \approx k_{z0} + \left.\frac{dk_{z_s}}{ds}\right|_{s_0}\Delta s\,(\mathbf{m}-\mathbf{h}) + \left.\frac{dk_{z_r}}{ds}\right|_{s_0}\Delta s\,(\mathbf{m}+\mathbf{h})\ , \tag{18}$$

where the depth wavenumber in the background medium is

$$\begin{aligned} k_{z0} &= \sqrt{\left[\omega s_0\,(\mathbf{m}-\mathbf{h})\right]^2 - \left|\frac{\mathbf{k_m}-\mathbf{k_h}}{2}\right|^2} \\ &+ \sqrt{\left[\omega s_0\,(\mathbf{m}+\mathbf{h})\right]^2 - \left|\frac{\mathbf{k_m}+\mathbf{k_h}}{2}\right|^2}\ . \end{aligned} \tag{19}$$

Here, $s_0\,(\mathbf{m})$ represents the spatially-variable *background* slowness at depth level z. Using the wavenumber linearization given by equation 18, we can reconstruct the acoustic wavefields in the background model using a phase-shift operation

$$u_{z+\Delta z}\,(\mathbf{m},\mathbf{h}) = e^{-ik_{z0}\Delta z}u_z\,(\mathbf{m},\mathbf{h})\ . \tag{20}$$

We can represent wavefield extrapolation using a generic solution to the one-way wave-equation using the notation $u_{z+\Delta z}\,(\mathbf{m},\mathbf{h}) = \mathcal{E}^{-}_{SSM}\left[s_{0z}\,(\mathbf{m}),u_z\,(\mathbf{m},\mathbf{h})\right]$. This notation indicates that the wavefield $u_{z+\Delta z}\,(\mathbf{m},\mathbf{h})$ is reconstructed from the wavefield $u_z\,(\mathbf{m},\mathbf{h})$ using the background slowness $s_0\,(\mathbf{m})$. This operation is repeated independently for all frequencies ω. A typical implementation of survey-sinking wave-equation migration uses the following algorithm:

SURVEY-SINKING MIGRATION ALGORITHM

$\omega = \omega_{min}\ldots\omega_{max}\{$
read $u\,(\mathbf{m},\mathbf{h})$
$z = z_{min}\ldots z_{max}\{$
write $u\,(\mathbf{m},\mathbf{h})$
read $r\,(\mathbf{m},\mathbf{h})$
$r\,(\mathbf{m},\mathbf{h}) += u\,(\mathbf{m},\mathbf{h})$
write $r\,(\mathbf{m},\mathbf{h})$
$u\,(\mathbf{m},\mathbf{h}) = \mathcal{E}^{-}_{SSM}\left[s_0\,(\mathbf{m}),u\,(\mathbf{m},\mathbf{h})\right]$

```
    }
}
```

This algorithm is similar to the one described in the preceding section for zero-offset migration, except that the wavefield and image are parametrized by midpoint and half-offset coordinates and that the depth wavenumber used in the extrapolation operator is given by the DSR equation using the background slowness $s_0(\mathbf{m})$. Wavefield extrapolation is usually implemented in a mixed domain (space-wavenumber), as briefly summarized in Appendix A.

Similarly to the derivation of the wavefield perturbation in the zero-offset migration case, we can write the linearized wavefield perturbation for survey-sinking migration as

$$\begin{aligned}
\Delta u(\mathbf{m},\mathbf{h}) \approx & - i \left.\frac{dk_{z_s}}{ds}\right|_{s_0} \Delta s(\mathbf{m}-\mathbf{h})\, \Delta z\, u(\mathbf{m},\mathbf{h}) \\
& - i \left.\frac{dk_{z_r}}{ds}\right|_{s_0} \Delta s(\mathbf{m}+\mathbf{h})\, \Delta z\, u(\mathbf{m},\mathbf{h}) \\
\approx & - i\Delta z \frac{\omega u(\mathbf{m},\mathbf{h})\, \Delta s(\mathbf{m}-\mathbf{h})}{\sqrt{1-\left[\frac{|\mathbf{k_m}-\mathbf{k_h}|}{2\omega s_0(\mathbf{m}-\mathbf{h})}\right]^2}} \\
& - i\Delta z \frac{\omega u(\mathbf{m},\mathbf{h})\, \Delta s(\mathbf{m}+\mathbf{h})}{\sqrt{1-\left[\frac{|\mathbf{k_m}+\mathbf{k_h}|}{2\omega s_0(\mathbf{m}+\mathbf{h})}\right]^2}} \; . \qquad (21)
\end{aligned}$$

Equation 21 defines the forward scattering operator $\mathcal{F}^{-}_{SSM}[u(\mathbf{m},\mathbf{h}), s_0(\mathbf{m}), \Delta s(\mathbf{m},\mathbf{h})]$, producing the scattered wavefield $\Delta u(\mathbf{m},\mathbf{h})$ from the slowness perturbation $\Delta s(\mathbf{m})$, based on the background slowness $s_0(\mathbf{m})$ and background wavefield $u(\mathbf{m},\mathbf{h})$. The image perturbation at depth z is obtained from the scattered wavefield using the time $t=0$ imaging condition, similar to the procedure used for imaging in the background medium:

$$\Delta r(\mathbf{m},\mathbf{h}) = \sum_{\omega} \Delta u(\mathbf{m},\mathbf{h},\omega) \; . \qquad (22)$$

Given an image perturbation $\Delta r(\mathbf{m},\mathbf{h})$, we can construct the scattered wavefield by the adjoint of the imaging condition

$$\Delta u(\mathbf{m},\mathbf{h},\omega) = \Delta r(\mathbf{m},\mathbf{h}) \; , \qquad (23)$$

for every frequency ω. Then, similarly to the procedure used in the zero-offset case, the slowness perturbation at depth z caused by a wavefield perturbation at depth z under the influence of the background wavefield at the same depth z can be written as

$$\begin{aligned}
\Delta s(\mathbf{m}-\mathbf{h}) \approx & + i \left.\frac{dk_{z_s}}{ds}\right|_{s_0} \Delta z\, \overline{u(\mathbf{m},\mathbf{h})} \Delta u(\mathbf{m},\mathbf{h}) \\
\approx & + i\Delta z \frac{\omega \overline{u(\mathbf{m},\mathbf{h})} \Delta u(\mathbf{m},\mathbf{h})}{\sqrt{1-\left[\frac{|\mathbf{k_m}-\mathbf{k_h}|}{2\omega s_0(\mathbf{m}-\mathbf{h})}\right]^2}} \; , \qquad (24)
\end{aligned}$$

and

$$\begin{aligned}
\Delta s(\mathbf{m}+\mathbf{h}) \approx & + i \left.\frac{dk_{z_r}}{ds}\right|_{s_0} \Delta z\, \overline{u(\mathbf{m},\mathbf{h})} \Delta u(\mathbf{m},\mathbf{h}) \\
\approx & + i\Delta z \frac{\omega \overline{u(\mathbf{m},\mathbf{h})} \Delta u(\mathbf{m},\mathbf{h})}{\sqrt{1-\left[\frac{|\mathbf{k_m}+\mathbf{k_h}|}{2\omega s_0(\mathbf{m}+\mathbf{h})}\right]^2}} \; . \qquad (25)
\end{aligned}$$

Equations 24-25 define the adjoint scattering operator $\mathcal{A}^{+}_{SSM}[u(\mathbf{m},\mathbf{h}), s_0(\mathbf{m}), \Delta u(\mathbf{m},\mathbf{h})]$, producing the slowness perturbation $\Delta s(\mathbf{m})$ from the scattered wavefield $\Delta u(\mathbf{m},\mathbf{h})$, based on the background slowness $s_0(\mathbf{m})$ and background wavefield $u(\mathbf{m},\mathbf{h})$. A typical implementation of survey-sinking forward and adjoint scattering follows the algorithms:

SURVEY-SINKING FORWARD SCATTERING ALGORITHM

```
ω = ω_min ... ω_max {
    initialize Δu(m,h) = 0
    z = z_min ... z_max {
        read u(m,h)
        read Δs(m)
        Δu(m,h) += F⁻_SSM [u(m,h), s0(m-h), Δs(m-h)]
        Δu(m,h) += F⁻_SSM [u(m,h), s0(m+h), Δs(m+h)]
        read Δr(m,h)
        Δr(m,h) += Δu(m,h)
        write Δr(m,h)
        Δu(m,h) = E⁻_SSM [s0(m), Δu(m,h)]
    }
}
```

SURVEY-SINKING ADJOINT SCATTERING ALGORITHM

```
ω = ω_min ... ω_max {
    initialize Δu(m,h) = 0
    z = z_max ... z_min {
        read u(m,h)
        Δu(m,h) = E⁺_SSM [s0(m), Δu(m,h)]
        read Δr(m,h)
        Δu(m,h) += Δr(m,h)
        read Δs(m)
        Δs(m-h) += A⁺_SSM [u(m,h), s0(m-h), Δu(m,h)]
        Δs(m+h) += A⁺_SSM [u(m,h), s0(m+h), Δu(m,h)]
        write Δs(m)
    }
}
```

These algorithms are similar to the ones described in the preceding section for zero-offset migration, except that the wavefield and image are parametrized by midpoint and half-offset coordinates. Furthermore, the two square-roots corresponding to the DSR equation update the slowness model separately, thus characterizing the source and receiver propagation paths to the image positions. Both forward and adjoint scattering algorithms require the background wavefield, $u(\mathbf{m},\mathbf{h})$, to be precomputed at all depth levels. Scattering and

wavefield extrapolation are implemented in the mixed space-wavenumber domain, as briefly explained in Appendix A.

2. 3 Shot-record migration and velocity analysis

Wavefield reconstruction for multi-offset migration based on the one-way wave-equation under the shot-record framework is performed by separate recursive extrapolation of the source and receiver wavefields, u_s and u_r. The wavefield extrapolation progresses forward in time (causal) for the source wavefield and backward in time (anti-causal) for the receiver wavefield:

$$u_{s\,z+\Delta z}\left(\mathbf{m}\right) = e^{+ik_z\Delta z}u_{s\,z}\left(\mathbf{m}\right) \tag{26}$$

$$u_{r\,z+\Delta z}\left(\mathbf{m}\right) = e^{-ik_z\Delta z}u_{r\,z}\left(\mathbf{m}\right) \tag{27}$$

In equations 26-27, $u_{s\,z}\left(\mathbf{m}\right)$ and $u_{r\,z}\left(\mathbf{m}\right)$ represent the source and receiver acoustic wavefield for a given frequency ω at all positions in space $\mathbf{m}$ at depth z, and $u_{s\,z+\Delta z}\left(\mathbf{m}\right)$ and $u_{r\,z+\Delta z}\left(\mathbf{m}\right)$ represent the same wavefields extrapolated to depth $z+\Delta z$. The phase shift operation uses the depth wavenumber k_z which is defined by the single square-root (SSR) equation

$$k_z = \sqrt{\left[\omega s\left(\mathbf{m}\right)\right]^2 - \left|\mathbf{k_m}\right|^2} \tag{28}$$

The image is obtained from the extrapolated wavefields by selection of the zero cross-correlation lags in space of time between the source and receiver wavefields, an operation which is usually implemented as summation over frequencies:

$$r_z\left(\mathbf{m}\right) = \sum_{\omega} \overline{u_{s\,z}\left(\mathbf{m},\omega\right)} u_{r\,z}\left(\mathbf{m},\omega\right) \ . \tag{29}$$

An alternative imaging condition (Sava & Fomel, 2006) preserves the space and time cross-correlation lags in the image.

Linearizing the depth wavenumber given by the equation 28 relative to the background slowness $s_0\left(\mathbf{m}\right)$ similarly to the case case of zero-offset migration, we can reconstruct the acoustic wavefields in the background model using a phase-shift operation

$$u_{s\,z+\Delta z}\left(\mathbf{m}\right) = e^{+ik_{z0}\Delta z}u_{s\,z}\left(\mathbf{m}\right) \ , \tag{30}$$

$$u_{r\,z+\Delta z}\left(\mathbf{m}\right) = e^{-ik_{z0}\Delta z}u_{r\,z}\left(\mathbf{m}\right) \ , \tag{31}$$

which define the causal $\mathcal{E}^{+}_{SRM}\left[s_{0\,z}\left(\mathbf{m}\right), u_z\left(\mathbf{m}\right)\right]$ and the anti-causal $\mathcal{E}^{-}_{SRM}\left[s_{0\,z}\left(\mathbf{m}\right), u_z\left(\mathbf{m}\right)\right]$ wavefield extrapolation operators for shot-record migration constructed using the background slowness $s_0\left(\mathbf{m}\right)$ and producing the wavefields $u_{s\,z+\Delta z}\left(\mathbf{m}\right)$ and $u_{r\,z+\Delta z}\left(\mathbf{m}\right)$ at depth $z+\Delta z$ from the wavefields $u_{s\,z}\left(\mathbf{m}\right)$ and $u_{r\,z}\left(\mathbf{m}\right)$ at depth z, respectively. A typical implementation of shot-record wave-equation migration follows the algorithm:

SHOT-RECORD MIGRATION ALGORITHM

```
ω = ω_min ... ω_max {
    read u_s(m) and u_r(m)
    z = z_min ... z_max {
        write u_s(m) and u_r(m)
        read r(m)
        r(m) += conj(u_s(m)) u_r(m)
        write r(m)
        u_s(m) = E+_SRM [s_0(m), u_s(m)]
        u_r(m) = E-_SRM [s_0(m), u_r(m)]
    }
}
```

This algorithm is similar to the one used for zero-offset or survey sinking migration, except that the source and receiver wavefields are reconstructed separately using wavefield extrapolation. Unlike the zero-offset extrapolation operator, the shot-record extrapolation operator uses the background slowness s_0 since the operation involves sinking of the source and receiver wavefields from the surface toward the image positions. Wavefield extrapolation is usually implemented in a mixed domain (space-wavenumber), as briefly summarized in Appendix A.

Similarly to the derivation of the wavefield perturbation in the zero-offset migration case, we can write the linearized wavefield perturbation for shot-record migration as

$$\begin{aligned}\Delta u_s\left(\mathbf{m}\right) &\approx +i\left.\frac{dk_z}{ds}\right|_{s_0}\Delta z\ u_s\left(\mathbf{m}\right)\Delta s\left(\mathbf{m}\right) \\ &\approx +i\Delta z\frac{\omega u_s\left(\mathbf{m}\right)\Delta s\left(\mathbf{m}\right)}{\sqrt{1-\left[\frac{\left|\mathbf{k_m}\right|}{\omega s_0(\mathbf{m})}\right]^2}}\ ,\end{aligned} \tag{32}$$

and

$$\begin{aligned}\Delta u_r\left(\mathbf{m}\right) &\approx -i\left.\frac{dk_z}{ds}\right|_{s_0}\Delta z\ u_r\left(\mathbf{m}\right)\Delta s\left(\mathbf{m}\right) \\ &\approx -i\Delta z\frac{\omega u_r\left(\mathbf{m}\right)\Delta s\left(\mathbf{m}\right)}{\sqrt{1-\left[\frac{\left|\mathbf{k_m}\right|}{\omega s_0(\mathbf{m})}\right]^2}}\ .\end{aligned} \tag{33}$$

Equations 32-33 define the forward scattering operators $\mathcal{F}^{\pm}_{SRM}\left[u\left(\mathbf{m}\right), s_0\left(\mathbf{m}\right), \Delta s\left(\mathbf{m}\right)\right]$ producing the scattered wavefields $\Delta u\left(\mathbf{m}\right)$ from the slowness perturbation $\Delta s\left(\mathbf{m}\right)$, based on the background slowness $s_0\left(\mathbf{m}\right)$ and background wavefield $u\left(\mathbf{m}\right)$. In this case, the symbol u stands for either u_s or u_r, given the appropriate choice of sign in the forward scattering operator. The image perturbation at depth z is obtained from the source and receiver scattered wavefields using the relation

$$\Delta r\left(\mathbf{m}\right) = \sum_{\omega}\left(\overline{u_s\left(\mathbf{m},\omega\right)}\Delta u_r\left(\mathbf{m},\omega\right) + \overline{\Delta u_s\left(\mathbf{m},\omega\right)}u_r\left(\mathbf{m},\omega\right)\right) \ , \tag{34}$$

which corresponds to the frequency-domain zero-lag cross-correlation of the source and receiver wavefields required by the imaging condition.

Given an image perturbation Δr, we can construct the scattered source and receiver wavefields by the adjoint of the imaging condition

$$\Delta u_s\left(\mathbf{m}\right) = u_r\left(\mathbf{m}\right)\overline{\Delta r\left(\mathbf{m}\right)} \ , \tag{35}$$

$$\Delta u_r\left(\mathbf{m}\right) = u_s\left(\mathbf{m}\right)\Delta r\left(\mathbf{m}\right) \ , \tag{36}$$

for every frequency ω. Then, the slowness perturbations due to the source and receiver wavefields at depth z under the influ-

ence of the background source and receiver wavefields at the same depth z can be written as

$$\begin{aligned}\Delta s_s(\mathbf{m}) &\approx -i\left.\frac{dk_z}{ds}\right|_{s_0}\Delta z\,\overline{u_s(\mathbf{m})}\Delta u_s(\mathbf{m}) \\ &\approx -i\Delta z\frac{\omega\overline{u_s(\mathbf{m})}\Delta u_s(\mathbf{m})}{\sqrt{1-\left[\frac{|\mathbf{k_m}|}{\omega s_0(\mathbf{m})}\right]^2}}\,, \end{aligned} \tag{37}$$

and

$$\begin{aligned}\Delta s_r(\mathbf{m}) &\approx -i\left.\frac{dk_z}{ds}\right|_{s_0}\Delta z\,\overline{u_r(\mathbf{m})}\Delta u_r(\mathbf{m}) \\ &\approx -i\Delta z\frac{\omega\overline{u_r(\mathbf{m})}\Delta u_r(\mathbf{m})}{\sqrt{1-\left[\frac{|\mathbf{k_m}|}{\omega s_0(\mathbf{m})}\right]^2}}\,. \end{aligned} \tag{38}$$

Equations 37-38 define the adjoint scattering operators $\mathcal{A}^{\pm}_{SRM}\left[u(\mathbf{m}), s_0(\mathbf{m}), \Delta u(\mathbf{m})\right]$, producing the slowness perturbation $\Delta s(\mathbf{m})$ from the scattered wavefield $\Delta u(\mathbf{m})$, based on the background slowness $s_0(\mathbf{m})$ and background wavefield $u(\mathbf{m})$. In this case, u stands for either u_s or u_r, given the appropriate choice of sign in the adjoint scattering operator. A typical implementation of shot-record forward and adjoint scattering follows the algorithms:

SHOT-RECORD FORWARD SCATTERING ALGORITHM

$\omega = \omega_{min} \dots \omega_{max}\{$
  initialize $\Delta u_s(\mathbf{m}) = 0$ and $\Delta u_r(\mathbf{m}) = 0$
  $z = z_{min} \dots z_{max}\{$
    read $u_s(\mathbf{m})$ and $u_r(\mathbf{m})$
    read $\Delta s(\mathbf{m})$
    $\Delta u_s(\mathbf{m}) += \mathcal{F}^{+}_{SRM}\left[u_s(\mathbf{m}), s_0(\mathbf{m}), \Delta s(\mathbf{m})\right]$
    $\Delta u_r(\mathbf{m}) += \mathcal{F}^{-}_{SRM}\left[u_r(\mathbf{m}), s_0(\mathbf{m}), \Delta s(\mathbf{m})\right]$
    read $\Delta r(\mathbf{m})$
    $\Delta r(\mathbf{m}) += \overline{u_s(\mathbf{m})}\Delta u_r(\mathbf{m})$
    $\Delta r(\mathbf{m}) += \overline{\Delta u_s(\mathbf{m})}u_r(\mathbf{m})$
    write $\Delta r(\mathbf{m})$
    $\Delta u_s(\mathbf{m}) = \mathcal{E}^{+}_{SRM}\left[s_0(\mathbf{m}), \Delta u_s(\mathbf{m})\right]$
    $\Delta u_r(\mathbf{m}) = \mathcal{E}^{-}_{SRM}\left[s_0(\mathbf{m}), \Delta u_r(\mathbf{m})\right]$
  $\}$
$\}$

SHOT-RECORD ADJOINT SCATTERING ALGORITHM

$\omega = \omega_{min} \dots \omega_{max}\{$
  initialize $\Delta u_s(\mathbf{m}) = 0$ and $\Delta u_r(\mathbf{m}) = 0$
  $z = z_{max} \dots z_{min}\{$
    read $u_s(\mathbf{m})$ and $u_r(\mathbf{m})$
    $\Delta u_r(\mathbf{m}) = \mathcal{E}^{+}_{SRM}\left[s_0(\mathbf{m}), \Delta u_r(\mathbf{m})\right]$
    $\Delta u_s(\mathbf{m}) = \mathcal{E}^{-}_{SRM}\left[s_0(\mathbf{m}), \Delta u_s(\mathbf{m})\right]$
    read $\Delta r(\mathbf{m})$
    $\Delta u_r(\mathbf{m}) += u_s(\mathbf{m})\,\Delta r(\mathbf{m})$
    $\Delta u_s(\mathbf{m}) += u_r(\mathbf{m})\,\overline{\Delta r(\mathbf{m})}$
    read $\Delta s(\mathbf{m})$
    $\Delta s(\mathbf{m}) += \mathcal{A}^{+}_{SRM}\left[u_r(\mathbf{m}), s_0(\mathbf{m}), \Delta u_r(\mathbf{m})\right]$
    $\Delta s(\mathbf{m}) += \mathcal{A}^{-}_{SRM}\left[u_s(\mathbf{m}), s_0(\mathbf{m}), \Delta u_s(\mathbf{m})\right]$
    write $\Delta s(\mathbf{m})$
  $\}$
$\}$

These algorithms are similar to the one used for zero-offset or survey sinking migration, except that the source and receiver wavefields are reconstructed separately using wavefield extrapolation. Unlike the zero-offset scattering operators, the shot-record scattering operators use the background slowness s_0 since the operation involves sinking of the source and receiver wavefields from the surface toward the image positions. Both forward and adjoint scattering algorithms require the background wavefields, $u_s(\mathbf{m})$ and $u_r(\mathbf{m})$, to be precomputed at all depth levels. Scattering and wavefield extrapolation are implemented in the mixed space-wavenumber domain, as briefly explained in Appendix A.

3 EXAMPLES

We illustrate the wave-equation migration velocity analysis operators using impulse responses corresponding to different imaging configurations. We concentrate on imaging in the zero-offset and shot-record frameworks, since they also implicitly characterize the essential elements of the survey-sinking framework. In all cases, we use wavefield reconstruction based on one-way wavefield extrapolation with the multi-reference split-step Fourier method (Stoffa *et al.*, 1990; Popovici, 1996).

A fundamental question concerning the wavefield scattering operator (W.S.) is what is its sensitivity for a given perturbation of the image or of the slowness model. This sensitivity is usually characterized using the so-called "sensitivity kernels" which are often discussed in the literature in the context of tomography problems. For wave-equation MVA, this topic was discussed in the context of zero-offset imaging by Sava & Biondi (2004a,b). The important topic of sensitivity and model resolution falls outside the scope of this paper, so we do not discuss it here in any detail. We merely concern ourselves with describing the behavior of the wave-equation MVA operators described earlier.

We can analyze the sensitivity of the wavefield scattering operator in two ways. The first option is to assume a localized slowness perturbation, compute image perturbations using the forward scattering operator and then return to the slowness perturbation using the adjoint scattering operator. The second option is to assume a localized image perturbation, compute the slowness perturbation using the adjoint scattering operator and then return to the image perturbation using the forward scattering operator.

As discussed in the preceding sections, the main difference between ray-based and wave-based MVA techniques is that the connection between measurements on the image and updates to the model is done with rays and waves, respectively. The impact of this fundamental difference is best seen if we analyze impulse responses of the wave-equation MVA

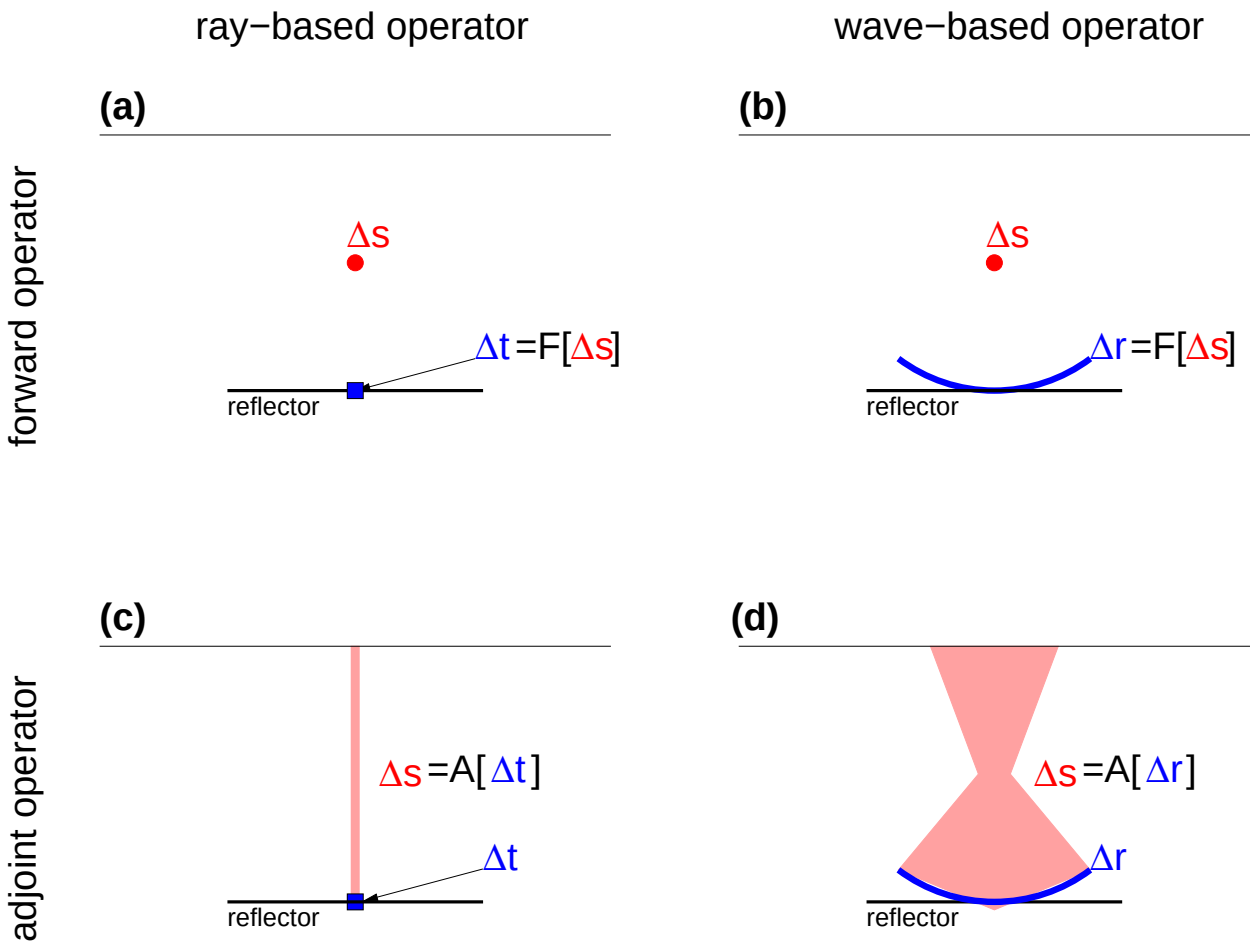

Figure 1. Schematic representation of the forward and adjoint operators for ray-based MVA and wave-based MVA. The forward operator F applied to a slowness anomaly Δs generates a traveltime perturbation (a) or an image perturbation (b). The ray-based adjoint MVA operator A applied to the traveltime perturbation generates a slowness perturbation uniformly distributed along a ray normal to the reflector (c). The wave-based adjoint MVA operator A applied to the image perturbation generates a slowness perturbation with a wider space distribution but with a relative focus at the location of the original slowness anomaly (d).

and compare them with those of conventional traveltime tomography. Figure 1 shows a one-to-one comparison between the forward and adjoint operators for ray-based MVA (traveltime tomography) on the left and wave-based MVA on the right in the context of zero-offset imaging. Assuming a small slowness perturbation Δs, we can construct using the forward MVA operators a traveltime perturbation and an image perturbation corresponding to ray-based MVA (a) and wave-based MVA (b), respectively. For this zero-offset configuration, the ray-based MVA produces a traveltime anomaly strictly located on the reflector under the slowness anomaly, while the wave-based MVA produces an image anomaly distributed in space in the vicinity of the reflector. Then, we can construct respective slowness updates if we apply the ray-based and wave-based adjoint MVA operators to the traveltime perturbation and image perturbation, respectively. For the ray-based MVA, the slowness update spreads uniformly along a ray orthogonal to the reflector (c), while for wave-based MVA, the slowness update is distributed in space from the image perturbation to the surface, but with a concentration at the location of the true anomaly (d). Similar behavior characterizes wave-equation MVA under shot-record or survey-sinking frameworks.

The first set of examples corresponds to a simple model consisting of a linear $v(z)$ velocity model and a horizontal reflector, Figures 2(a)-2(b). The velocity is linearly increasing from 1.5 km/s to 2.75 km/s. We simulate zero-offset data, Figure 4(a), and one shot corresponding to horizontal position $x = 6$ km, Figure 4(b).

Assuming a localized slowness perturbation, Figure 3(a), we can compute image perturbations using the forward scattering operators, as defined in the preceding sections. Figure 5(a) shows the image perturbation for the zero-offset case and Figure 6(a) shows the similar image perturbation for the shot-record case. As illustrated in Figure 1, the image perturbations are distributed in the vicinity of the reflector. Two interfering

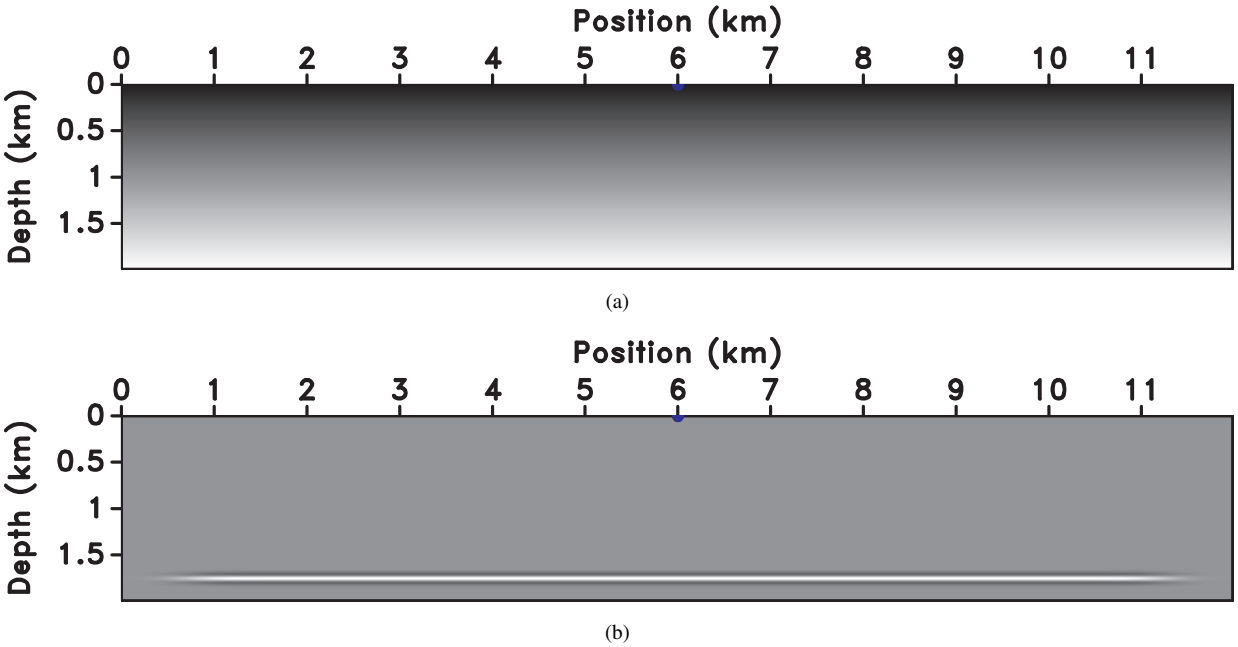

Figure 2. Simple synthetic model with (a) linear $v\,(z)$ velocity and (b) a horizontal reflector.

events are seen for the shot-record case, corresponding to the source and receiver wavefields, respectively.

Similarly, we can compute slowness perturbations using the adjoint scattering operators. Figure 5(b) shows the slowness perturbation for the zero-offset case computed from the image perturbation in Figure 5(a) and Figure 6(b) shows the similar slowness perturbation for the shot-record case computed from the image perturbation in Figure 6(a). As illustrated in Figure 1, the slowness perturbations are distributed in an area connecting the reflector to the surface, but with a relative focus at the location of the original anomaly. For the shot-record case, the back-projection splits toward the source and receivers, corresponding to the upward continuation of the source and receiver wavefields.

We can also analyze the wave-equation MVA operator sensitivity in another way. Assuming a localized image perturbation, Figure 3(b), we can compute slowness perturbations using the adjoint scattering operators, as defined in the preceding sections. Figure 7(a) shows the slowness perturbation for the zero-offset case and Figure 8(a) shows the similar slowness perturbation for the shot-record case. Here, too, we see slowness perturbations distributed in an area connecting the reflector to the surface, but in this case, there is no relative focus of the anomaly because the image perturbation is strictly localized on the reflector. For the shot-record case, the back-projection splits toward the source and receivers, corresponding to the upward continuation of the source and receiver wavefields. This case corresponds to the case of practical MVA where measurements of defocusing features are made on the image itself.

As we have done in the preceding experiment, we can also compute image perturbations using the forward scattering operators based on the back-projections created using the adjoint scattering operators. Figure 7(b) shows the image perturbation for the zero-offset case computed from the slowness perturbation in Figure 7(a) and Figure 8(b) shows the similar image perturbation for the shot-record case computed from the slowness perturbation in Figure 8(a). We can observe that the resulting image perturbations spread beyond the original location, indicating wider sensitivity of the wave-based MVA kernels to image perturbations than that of the corresponding ray-based MVA kernels.

Similar sensitivity can be observed for the more complex Sigsbee 2A model (Paffenholz *et al.*, 2002), Figures 9(a)-9(b). Similarly to the preceding example, we simulate zero-offset data, Figure 11(a), and one shot corresponding to horizontal position $x = 14.6$ km, Figure 11(b).

Figures 12(a) and 13(a) correspond to the image perturbations for the slowness anomaly shown in Figure 10(a). We can observe image perturbations that spread in the vicinity of the reflector, similarly to the simpler example described earlier. The multi-pathing from the source to the reflector generates the multiple events characterizing the image perturbations. Figures 12(b) and 13(b) correspond to the slowness perturbations constructed by applying the zero-offset and shot-record adjoint scattering operators to the image perturbations from Figures 12(a) and 13(a). We see similar back-projection patterns to the ones observed in the preceding example, except that the propagation pattens are more complicated due to the presence of the salt body in the background model.

Figures 14(a) and 15(a) correspond to the slowness perturbations for the image anomaly shown in Figure 10(b). We

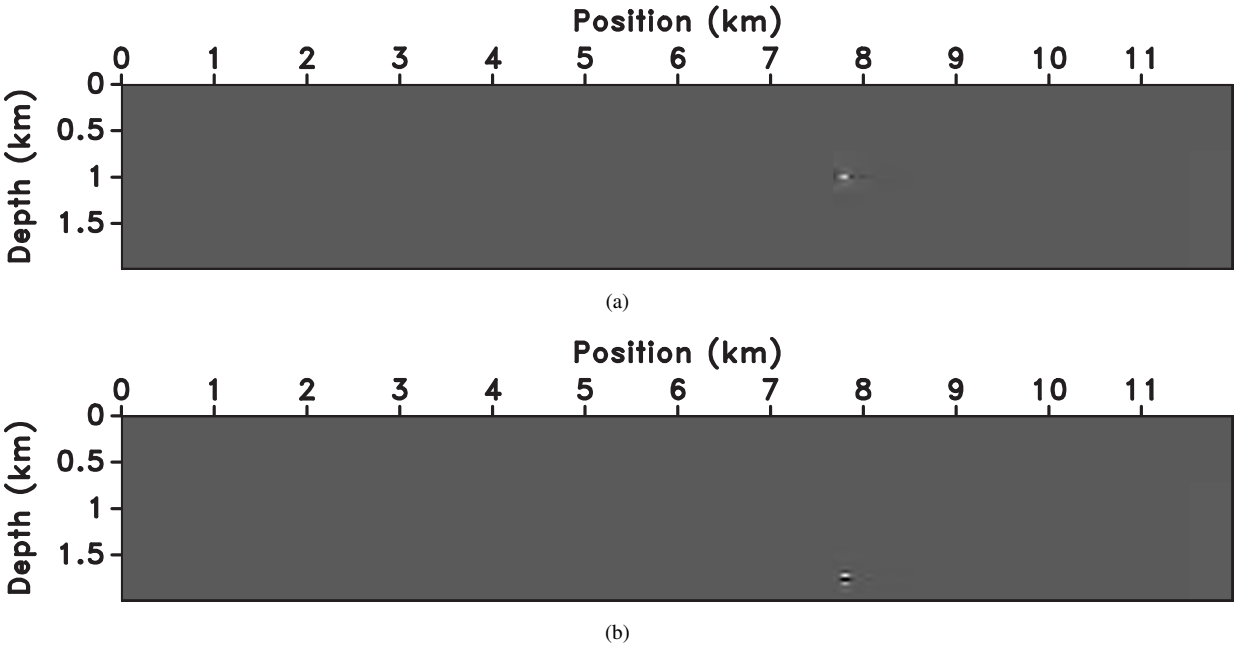

Figure 3. (a) Slowness perturbations used to demonstrate the WEMVA operators in Figures 5(a)-6(b), and (b) image perturbation used to demonstrate the WEMVA operators in Figures 7(a)-8(b).

can observe slowness perturbations that spread in the vicinity of the reflector, similarly to the simpler example described earlier. Finally, Figures 14(b) and 15(b) correspond to the image perturbations for the slowness perturbations constructed by the adjoint MVA operators shown in Figures 14(a) and 15(a) for the zero-offset and shot-record cases, respectively.

4 CONCLUSIONS

The wave-equation MVA operator discussed in this paper, can be implemented in various imaging frameworks, e.g. zero-offset (exploding reflector), survey-sinking or shot-record. In all cases, the forward and adjoint operators follow similar patterns involving combinations of scattering, imaging and extrapolation. The forward and adjoint operators share common elements and can be implemented in the mixed space-wavenumber domain, similarly to the implementation of the wavefield extrapolation operators.

The real challenges in using wave-based MVA are two-fold. First, the image perturbations need to be generated by techniques that do not compare image features that are too far from one-another, which is a property partially addressed by techniques based on differential semblance. Second, the cost of the wave-equation MVA operator is large, therefore a feasible implementation requires clever numeric implementation, e.g. by frequency decimation similarly to the approach taken in waveform inversion.

The examples shown in this paper illustrate the main characteristics of the various wave-equation MVA operators, i.e. stability during back-projection in background models with sharp velocity variation (e.g. salt), natural ability to characterize multi-pathing and wide area of sensitivity which is commensurate with the frequency band of the recorded data.

5 ACKNOWLEDGMENTS

This work is partially supported by the sponsors of the Center for Wave Phenomena at Colorado School of Mines and by a research grant from StatoilHydro.

REFERENCES

Al-Yahya, K., 1987, Velocity analysis by iterative profile migration: , PhD thesis, Stanford University.

Albertin, U., Sava, P., Etgen, J., and Maharramov, M., 2006a, Adjoint wave-equation velocity analysis: 74th Annual International Meeting, SEG, Expanded Abstracts, 3009–3013.

——— 2006b, Image differencing and focusing in wave-equation velocity analysis: 68th Mtg., Eur. Assoc. Expl. Geophys., Abstracts.

Albertin, U., 2006, Personal communication: Personal communication:.

Berkhout, A. J., 1982, Imaging of acoustic energy by wave field extrapolation: , Elsevier.

Billette, F., Begat, S. L., Podvin, P., and Lambare, G., 2003, Practical aspects and applications of 2D sterotomography: Geophysics, **68**, no. 3, 1008–1021.

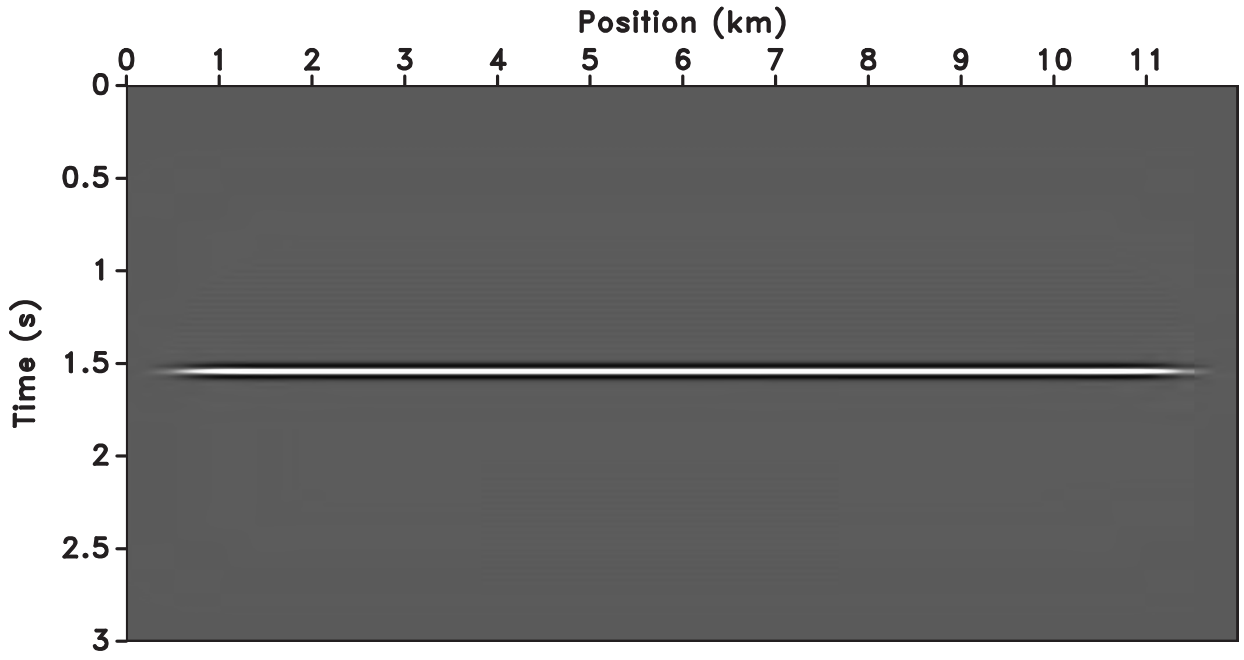

(a)

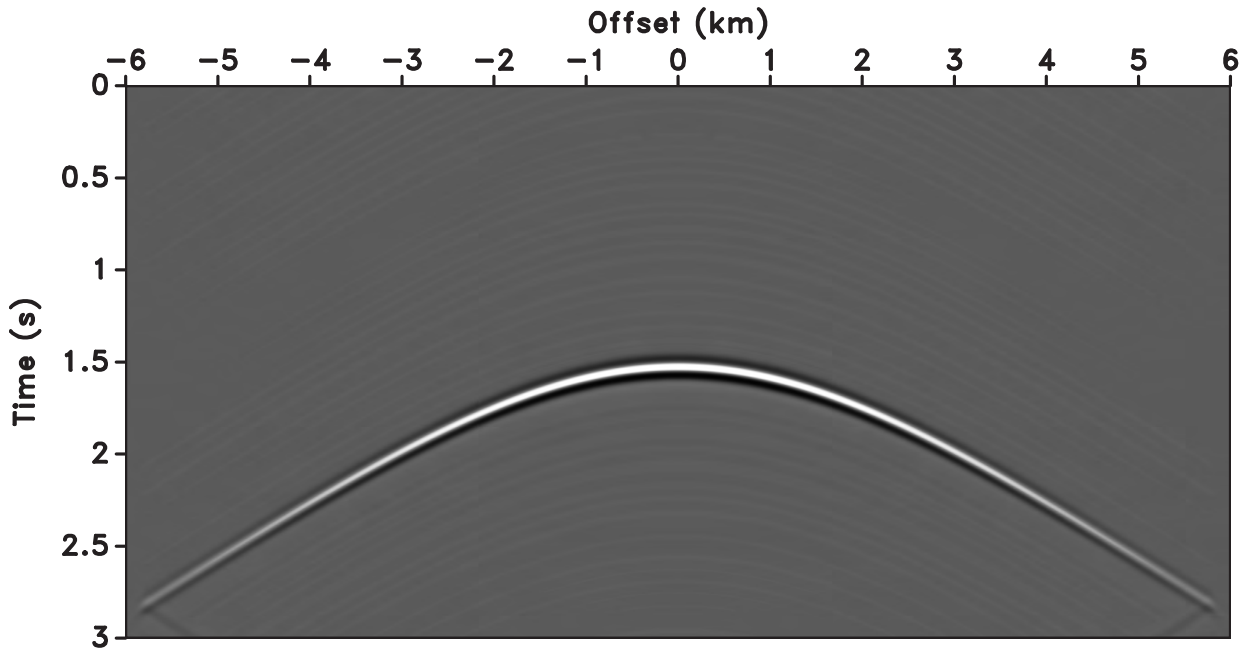

(b)

Figure 4. (a) Simulated zero-offset data and (b) simulated shot-record data for the model depicted in Figures 2(a)-2(b) with a source located at coordinates $x = 6$ km and $z = 0$ km.

Biondi, B., and Sava, P., 1999, Wave-equation migration velocity analysis: 69th Annual International Meeting, SEG, Expanded Abstracts, 1723–1726.

Biondi, B., and Symes, W., 2004, Angle-domain common-image gathers for migration velocity analysis by wavefield-continuation imaging: Geophysics, **69**, no. 5, 1283–1298.

Biondi, B., 2003, Equivalence of source-receiver migration and shot-profile migration: Geophysics, **68**, no. 4, 1340–1347.

Bishop, T. N., Bube, K. P., Cutler, R. T., Langan, R. T., Love,

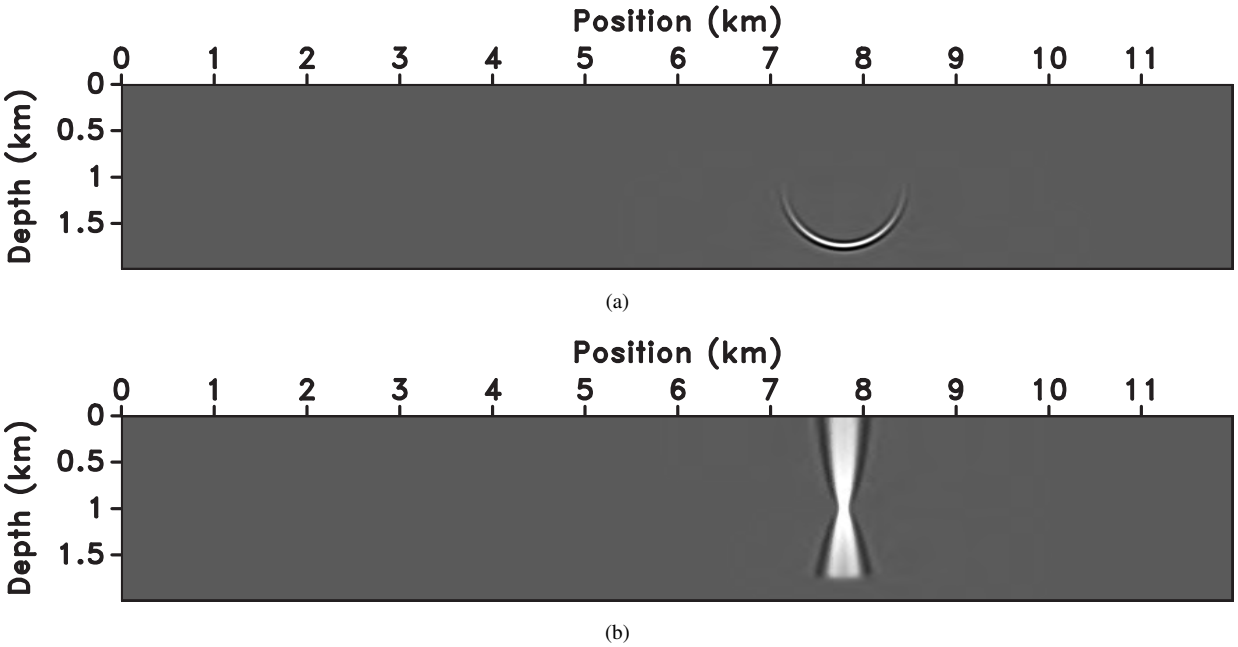

Figure 5. (a) Zero-offset image perturbation obtained by the application of the forward scattering operator to the slowness perturbation from Figure 3(a) and (b) zero-offset slowness perturbation obtained by the application of the adjoint scattering operator to the image perturbation from panel (a).

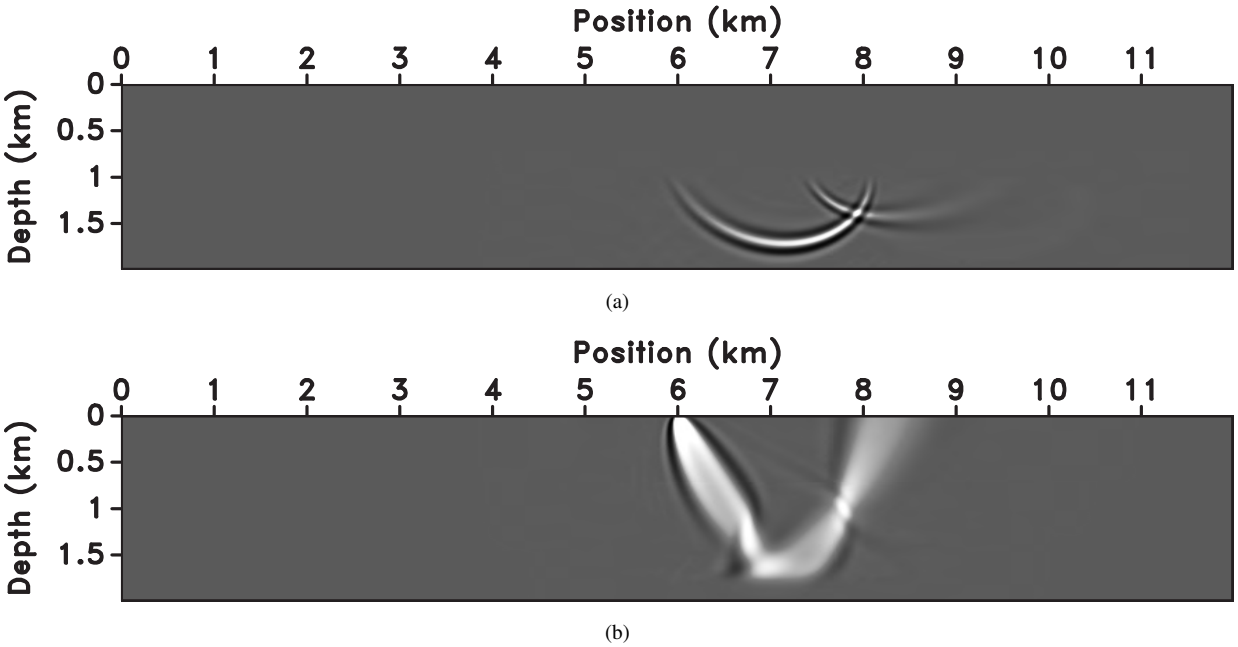

Figure 6. (a) Shot-record image perturbation obtained by the application of the forward scattering operator to the slowness perturbation from Figure 3(a) and (b) shot-record slowness perturbation obtained by the application of the adjoint scattering operator to the image perturbation from panel (a).

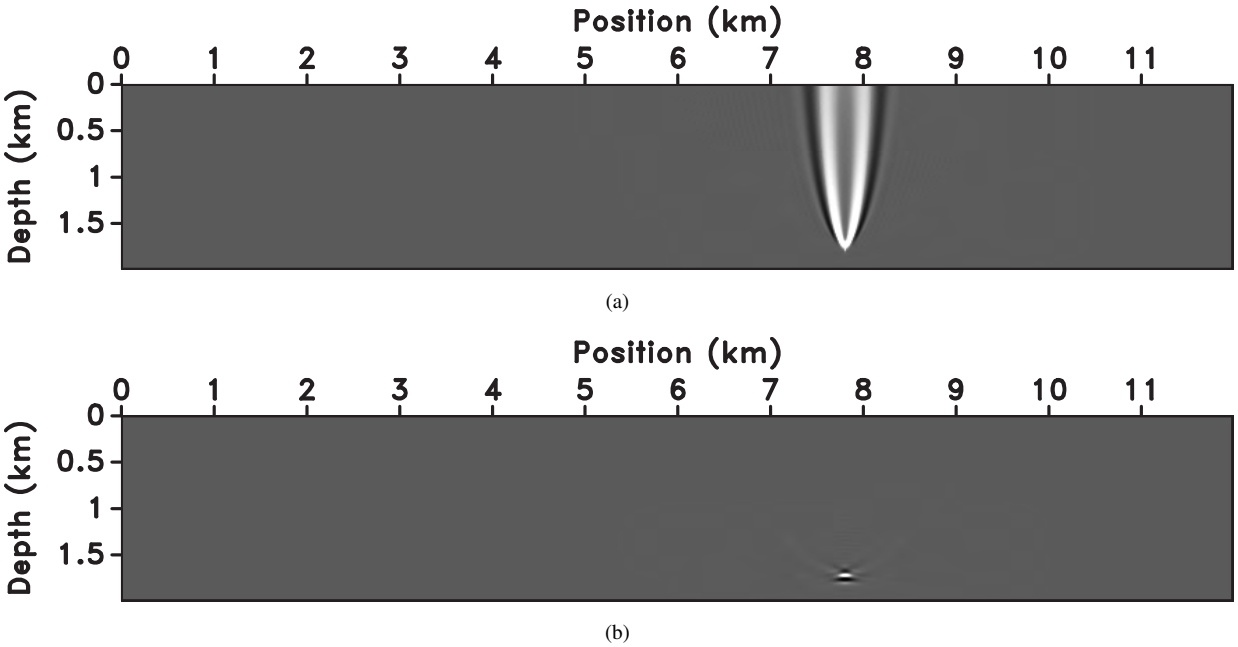

Figure 7. (a) Zero-offset slowness perturbation obtained by the application of the adjoint scattering operator to the image perturbation from Figure 3(b) and (b) zero-offset image perturbation obtained by the application of the forward scattering operator to the slowness perturbation from panel (a).

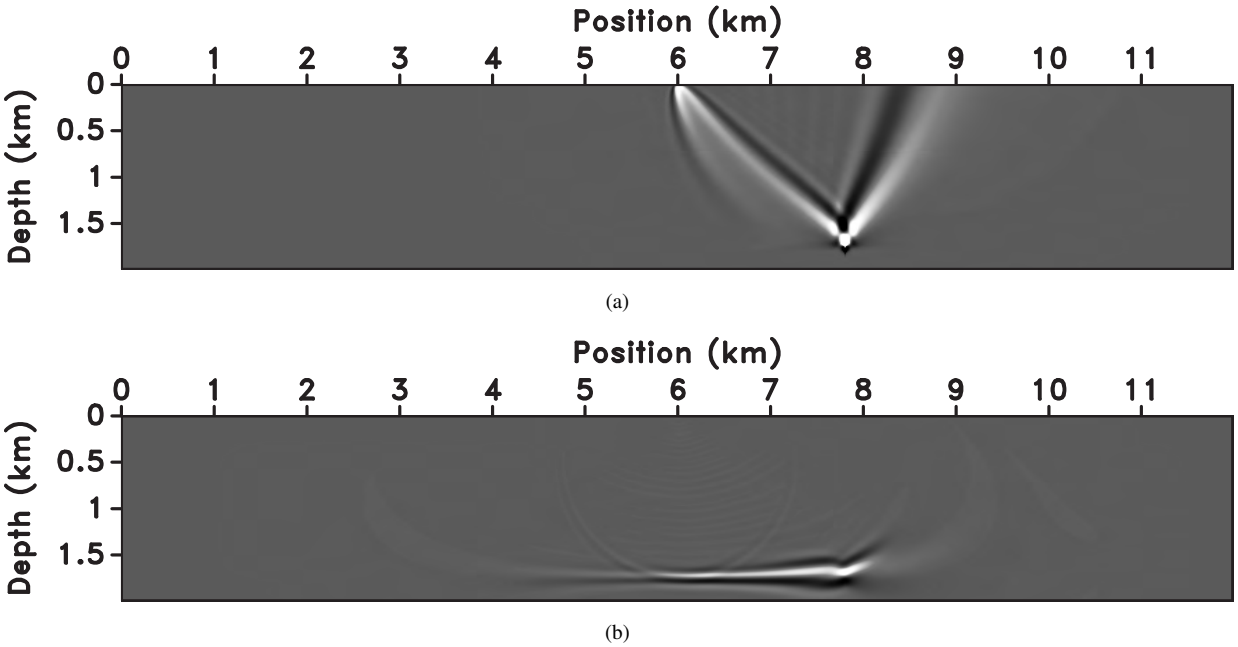

Figure 8. (a) Shot-record slowness perturbation obtained by the application of the adjoint scattering operator to the image perturbation from Figure 3(a) and (b) shot-record image perturbation obtained by the application of the forward scattering operator to the slowness perturbation from panel (a).

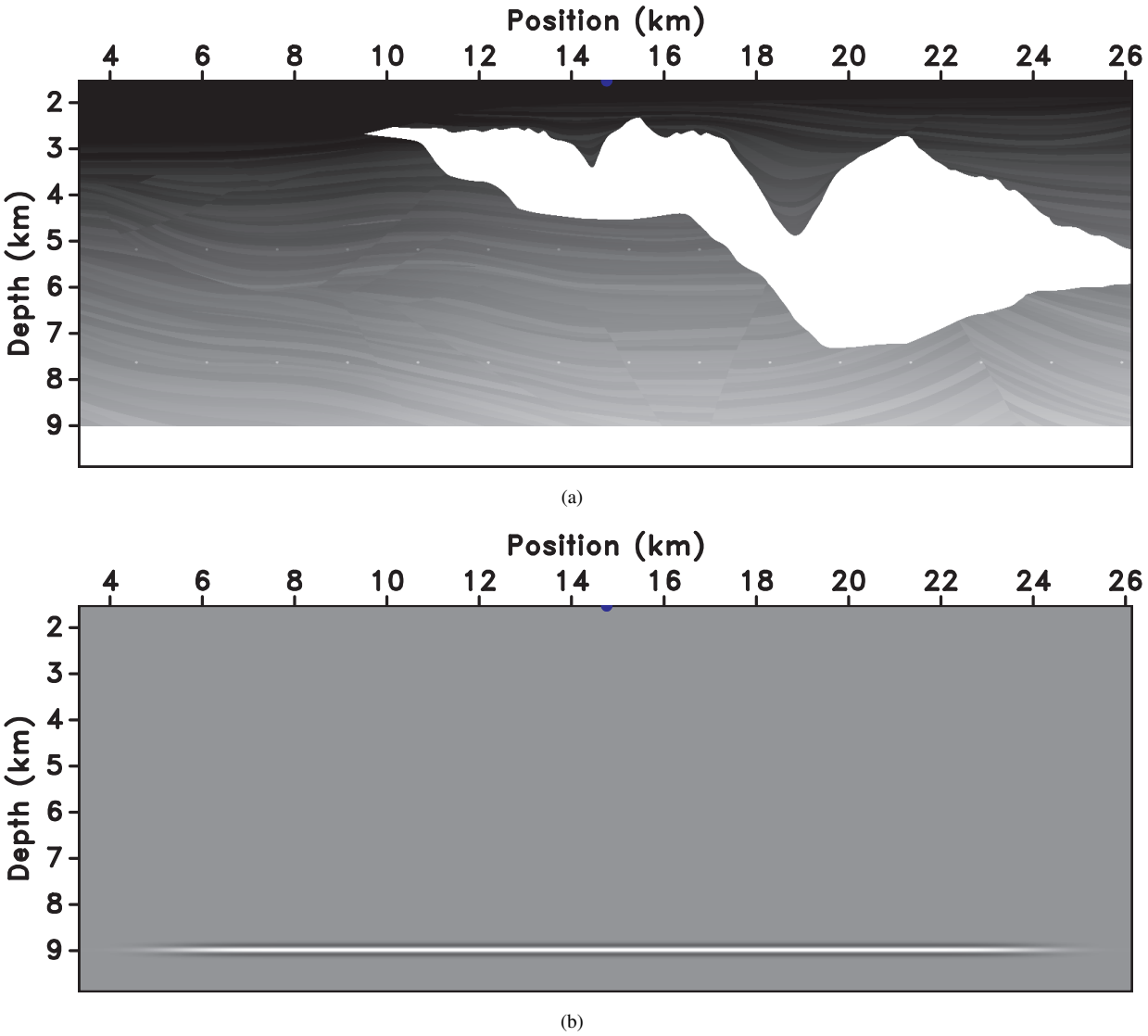

Figure 9. (a) Sigsbee 2A synthetic model and (b) a sub-salt horizontal reflector.

P. L., Resnick, J. R., Shuey, R. T., Spindler, D. A., and Wyld, H. W., 1985, Tomographic determination of velocity and depth in laterally varying media: Geophysics, **50**, no. 06, 903–923.

Chauris, H., Noble, M. S., Lambare, G., and Podvin, P., 2002a, Migration velocity analysis from locally coherent events in 2-D laterally heterogeneous media, Part I: Theoretical aspects: Geophysics, **67**, no. 04, 1202–1212.

——— 2002b, Migration velocity analysis from locally coherent events in 2-D laterally heterogeneous media, Part Ii: Applications on synthetic and real data: Geophysics, **67**, no. 04, 1213–1224.

Chavent, G., and Jacewitz, C. A., 1995, Determination of background velocities by multiple migration fitting: Geophysics, **60**, no. 02, 476–490.

Claerbout, J. F., 1985, Imaging the Earth's interior: , Blackwell Scientific Publications.

Clapp, R. G., Biondi, B., and Claerbout, J. F., 2004, Incorporating geologic information into reflection tomography: Geophysics, **69**, no. 2, 533–546.

Clement, F., Chavent, G., and Gomez, S., 2001, Migration-based traveltime waveform inversion of 2-D simple structures: A synthetic example: Geophysics, **66**, no. 3, 845–860.

de Bruin, C. G. M., Wapenaar, C. P. A., and Berkhout, A. J., 1990, Angle-dependent reflectivity by means of prestack migration: Geophysics, **55**, no. 09, 1223–1234.

Etgen, J., 1990, Residual prestack migration and interval-velocity estimation: , PhD thesis, Stanford University.

Fomel, S., 2004, Theory of 3-D angle gathers in wave-equation imaging: Expanded Abstracts.

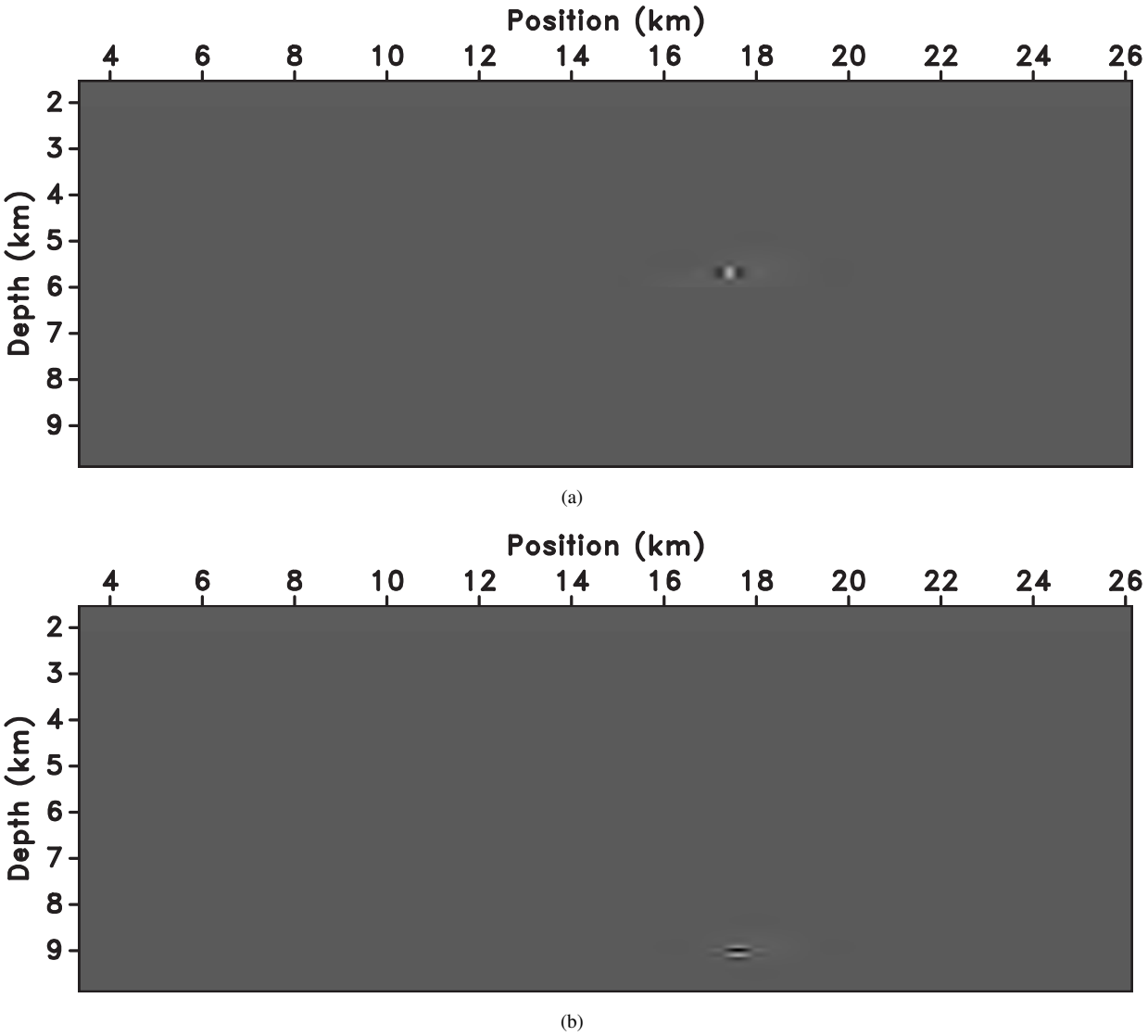

Figure 10. (a) Slowness perturbations used to demonstrate the WEMVA operators in Figures 12(a)-13(b), and (b) image perturbation used to demonstrate the WEMVA operators in Figures 14(a)-15(b).

Fowler, P., 1988, Seismic velocity estimation using prestack time migration: , PhD thesis, Stanford University.

Gauthier, O., Virieux, J., and Tarantola, A., 1986, Two-dimensional nonlinear inversion of seismic waveforms - Numerical results: Geophysics, **51**, no. 07, 1387–1403.

Huang, L. Y., Fehler, M. C., and Wu, R. S., 1999, Extended local Born Fourier migration method: Geophysics, **64**, no. 5, 1524–1534.

Lambare, G., Alerini, M., Baina, R., and Podvin, P., 2004, Stereotomography: a semi-automatic approach for velocity macromodel estimation: Geophys. Prosp., **52**, no. 6, 671–681.

Loewenthal, D., Lu, L., Roberson, R., and Sherwood, J., 1976, The wave equation applied to migration: Geophys. Prosp., **24**, no. 02, 380–399.

Maharramov, M., and Albertin, U., 2007, Localized image-difference wave-equation tomography: 75th Annual International Meeting, SEG, Expanded Abstracts.

Mora, P., 1989, Inversion = migration + tomography: Geophysics, **54**, no. 12, 1575–1586.

Mosher, C., and Foster, D., 2000, Common angle imaging conditions for prestack depth migration: Common angle imaging conditions for prestack depth migration:, Soc. of Expl. Geophys., 70th Ann. Internat. Mtg, 830–833.

Paffenholz, J., McLain, B., Zaske, J., and Keliher, P., 2002, Subsalt multiple attenuation and imaging: Observations from the Sigsbee2B synthetic dataset: Subsalt multiple attenuation and imaging: Observations from the Sigsbee2B

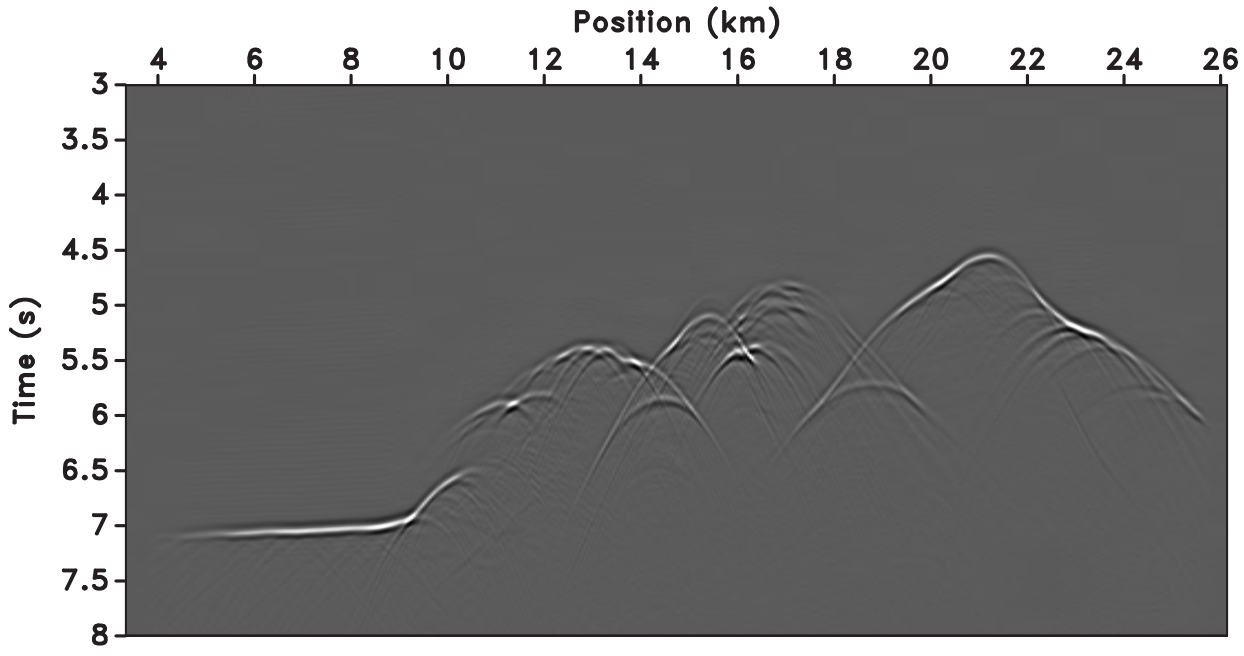

(a)

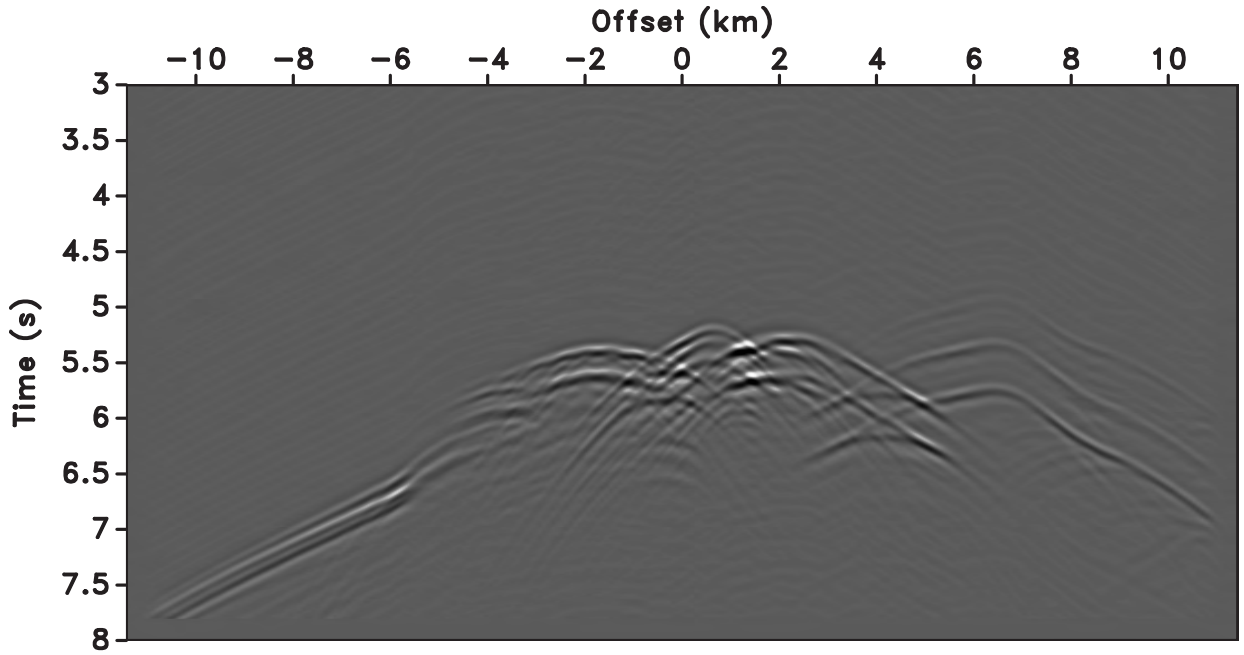

(b)

Figure 11. (a) Simulated zero-offset data and (b) simulated shot-record data for the model depicted in Figures 9(a)-9(b) with a source located at coordinates $x = 14.6$ km and $z = 1.52$ km.

synthetic dataset:, Soc. of Expl. Geophys., 72nd Annual International Meeting, SEG, 2122–2125.

Popovici, A. M., 1996, Prestack migration by split-step DsR: Geophysics, **61**, no. 05, 1412–1416.

Pratt, R. G., 1999, Seismic waveform inversion in the frequency domain, Part 1: Theory and verification in a physical scale model: Geophysics, **64**, no. 3, 888–901.

Pratt, R. G., 2004, Velocity models from frequency-domain waveform tomography: Past, present and future.: Velocity models from frequency-domain waveform tomography:

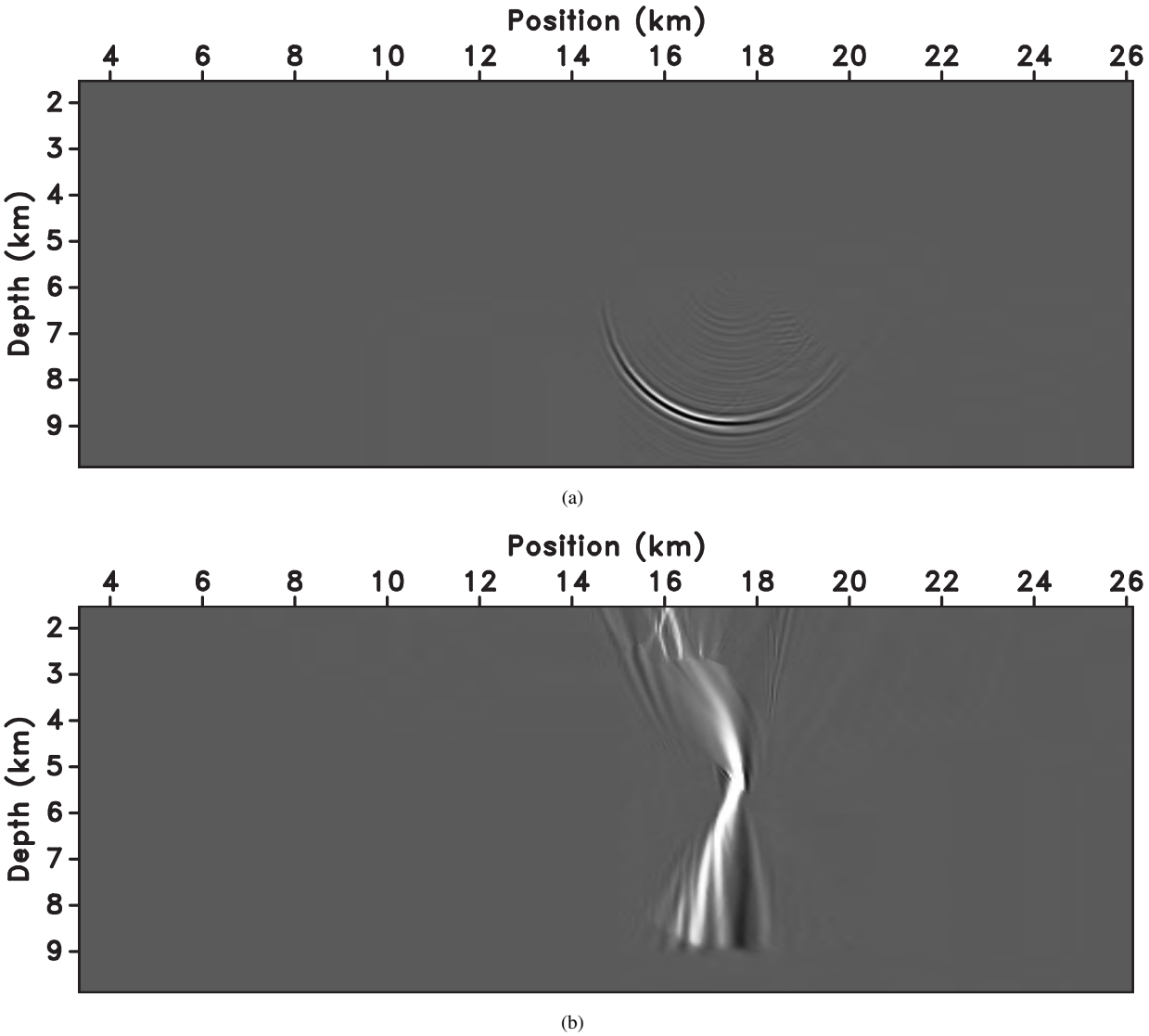

Figure 12. (a) Zero-offset image perturbation obtained by the application of the forward scattering operator to the slowness perturbation from Figure 10(a) and (b) zero-offset slowness perturbation obtained by the application of the adjoint scattering operator to the image perturbation from panel (a).

Past, present and future.:, EAGE, 66th Conference and Exhibition of the EAGE, Paris, France.

Prucha, M., Biondi, B., and Symes, W., 1999, Angle-domain common image gathers by wave-equation migration: Angle-domain common image gathers by wave-equation migration:, Soc. of Expl. Geophys., 69th Ann. Internat. Mtg, 824–827.

Rickett, J. E., and Sava, P. C., 2002, Offset and angle-domain common image-point gathers for shot-profile migration: Geophysics, **67**, no. 03, 883–889.

Ristow, D., and Ruhl, T., 1994, Fourier finite-difference migration: Geophysics, **59**, no. 12, 1882–1893.

Sava, P., and Biondi, B., 2004a, Wave-equation migration velocity analysis - I: Theory: Geophysical Prospecting, **52**, 593–606.

——— 2004b, Wave-equation migration velocity analysis - II: Subsalt imaging examples: Geophysical Prospecting, **52**, 607–623.

Sava, P. C., and Fomel, S., 2003, Angle-domain common-image gathers by wavefield continuation methods: Geophysics, **68**, no. 3, 1065–1074.

Sava, P., and Fomel, S., 2006, Time-shift imaging condition in seismic migration: Geophysics, **71**, no. 6, S209–S217.

Sava, P., Biondi, B., and Etgen, J., 2005, Wave-equation migration velocity analysis by focusing diffractions and reflections: Geophysics, **70**, U19–U27.

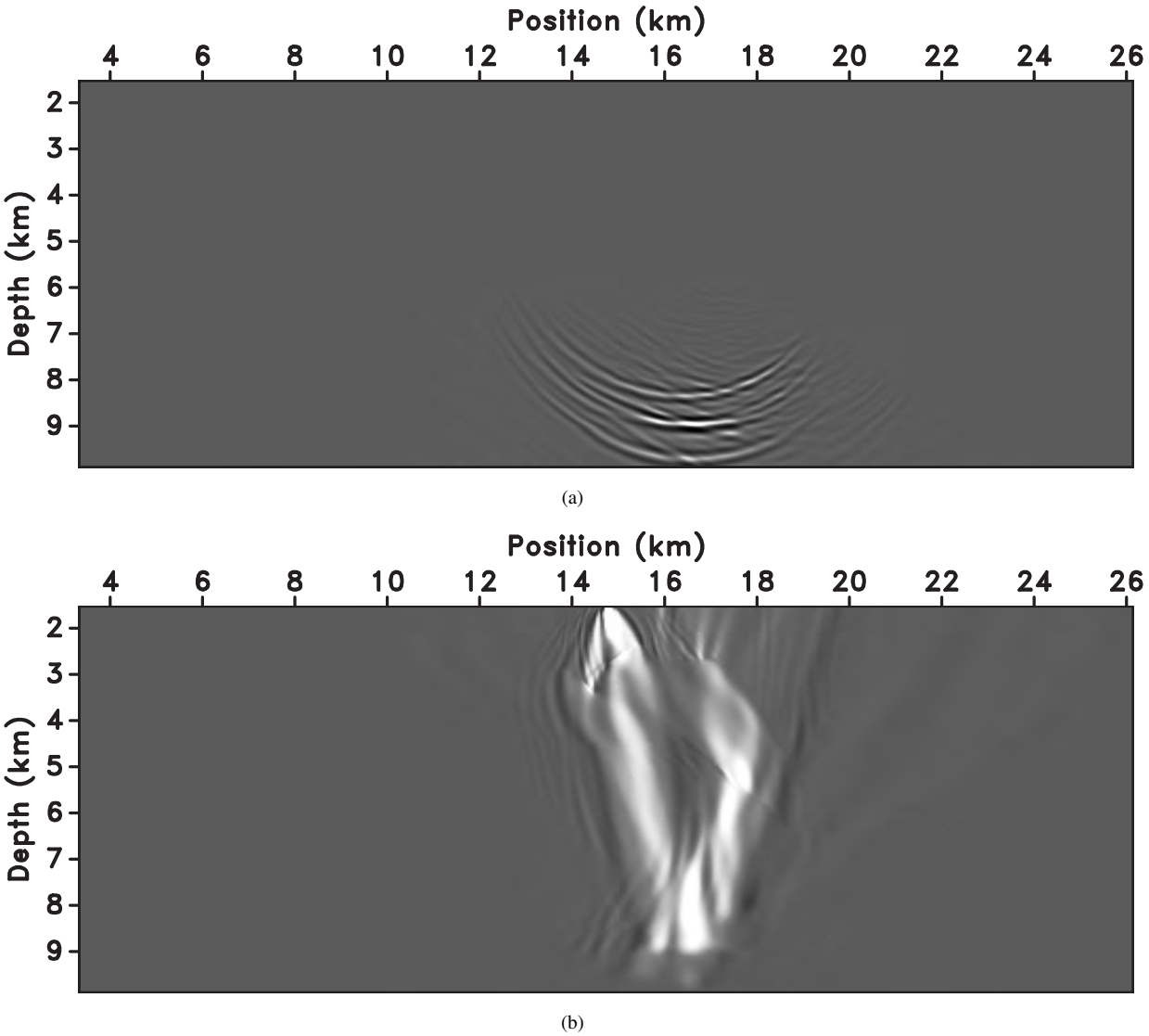

Figure 13. (a) Shot-record image perturbation obtained by the application of the forward scattering operator to the slowness perturbation from Figure 10(a) and (b) shot-record slowness perturbation obtained by the application of the adjoint scattering operator to the image perturbation from panel (a).

Shen, P., Symes, W., and Stolk, C. C., 2003, Differential semblance velocity analysis by wave-equation migration: Differential semblance velocity analysis by wave-equation migration:, Soc. of Expl. Geophys., 73rd Ann. Internat. Mtg., 2132–2135.

Shen, P., Symes, W., Morton, S., and Calandra, H., 2005, Differential semblance velocity analysis via shot profile migration: 75th Annual International Meeting, SEG, Expanded Abstracts, 2249–2252.

Sirgue, L., and Pratt, R., 2004, Efficient waveform inversion and imaging: A strategy for selecting temporal frequencies: Geophysics, **69**, no. 1, 231–248.

Soubaras, R., 2003, Angle gathers for shot-record migration by local harmonic decomposition: Angle gathers for shot-record migration by local harmonic decomposition:, Soc. of Expl. Geophys., 73rd Ann. Internat. Mtg., 889–892.

Stoffa, P. L., Fokkema, J. T., de Luna Freire, R. M., and Kessinger, W. P., 1990, Split-step Fourier migration: Geophysics, **55**, no. 04, 410–421.

Stolk, C. C., and Symes, W. W., 2004, Kinematic artifacts in prestack depth migration: Geophysics, **69**, no. 2, 562–575.

Stork, C., 1992, Reflection tomography in the postmigrated domain: Geophysics, **57**, no. 05, 680–692.

Symes, W. W., and Carazzone, J. J., 1991, Velocity inversion by differential semblance optimization: Geophysics, **56**, no. 05, 654–663.

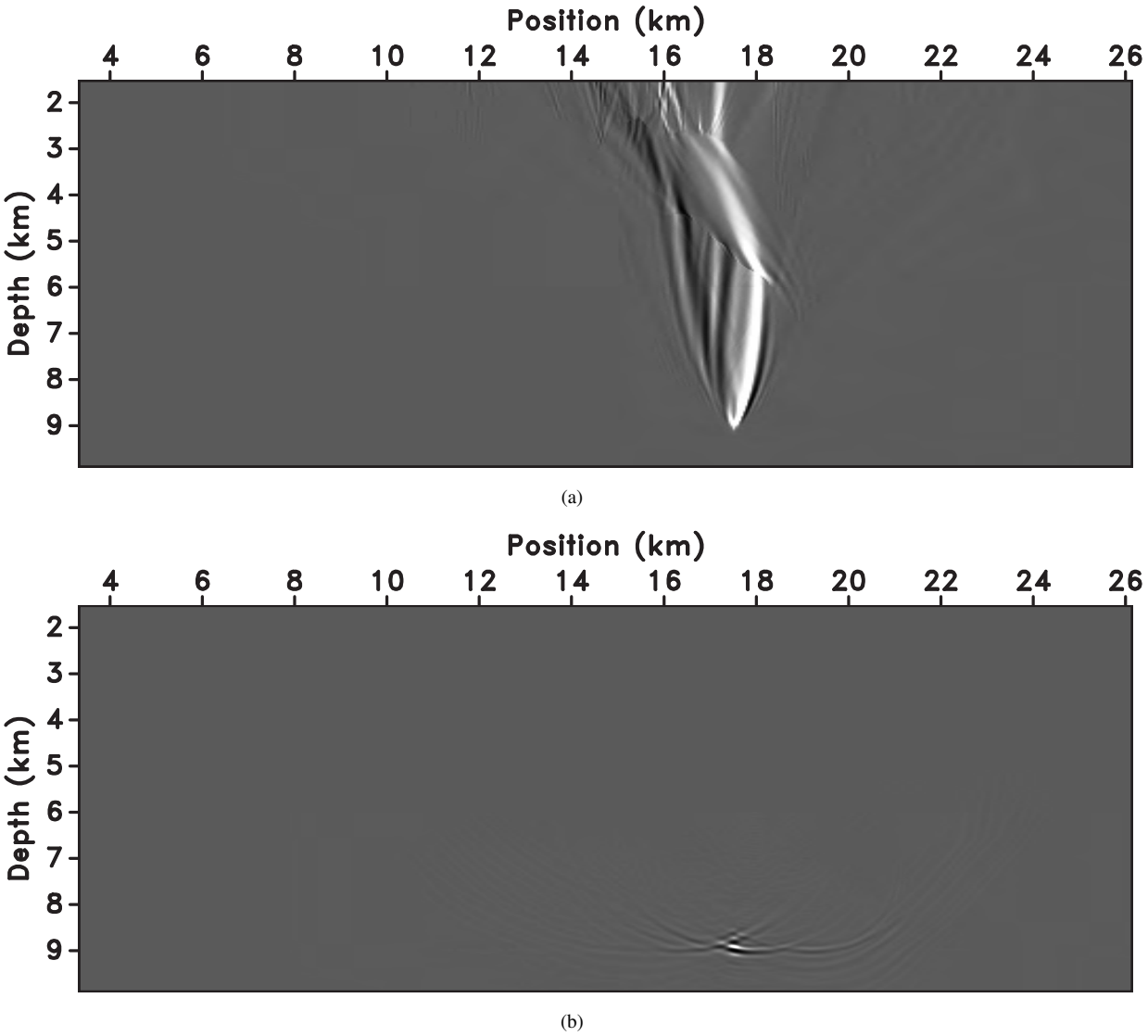

Figure 14. (a) Zero-offset slowness perturbation obtained by the application of the adjoint scattering operator to the image perturbation from Figure 10(b) and (b) zero-offset image perturbation obtained by the application of the forward scattering operator to the slowness perturbation from panel (a).

Tarantola, A., 1987, Inverse Problem Theory: methods for data fitting and model parameter estimation: , Elsevier.

Woodward, M. J., 1992, Wave-equation tomography: Geophysics, **57**, no. 01, 15–26.

Xie, X., and Wu, R., 2002, Extracting angle domain information from migrated wavefield: Expanded Abstracts, 1360–1363.

Yilmaz, O., and Chambers, R. E., 1984, Migration velocity analysis by wave-field extrapolation: Geophysics, **49**, no. 10, 1664–1674.

6 APPENDIX A: MIXED-DOMAIN OPERATORS

For the case of the phase-shift operation in media with lateral slowness variation, the mixed-domain solution involves forward and inverse Fourier transforms (denoted fFT and iFT in our algorithms) which can be implemented efficiently using standard Fast Fourier Transform algorithms. The numeric implementation is summarized in the following table:

MIXED-DOMAIN IMPLEMENTATION OF THE EXTRAPOLATION OPERATOR $\mathcal{E}^{\pm}_{ZOM}$ []

$u(\mathbf{m}) \xrightarrow{2D} u(\mathbf{k_m})$

$u(\mathbf{k_m}) * = e^{\pm i k_z \mathbf{k}} \Delta z$

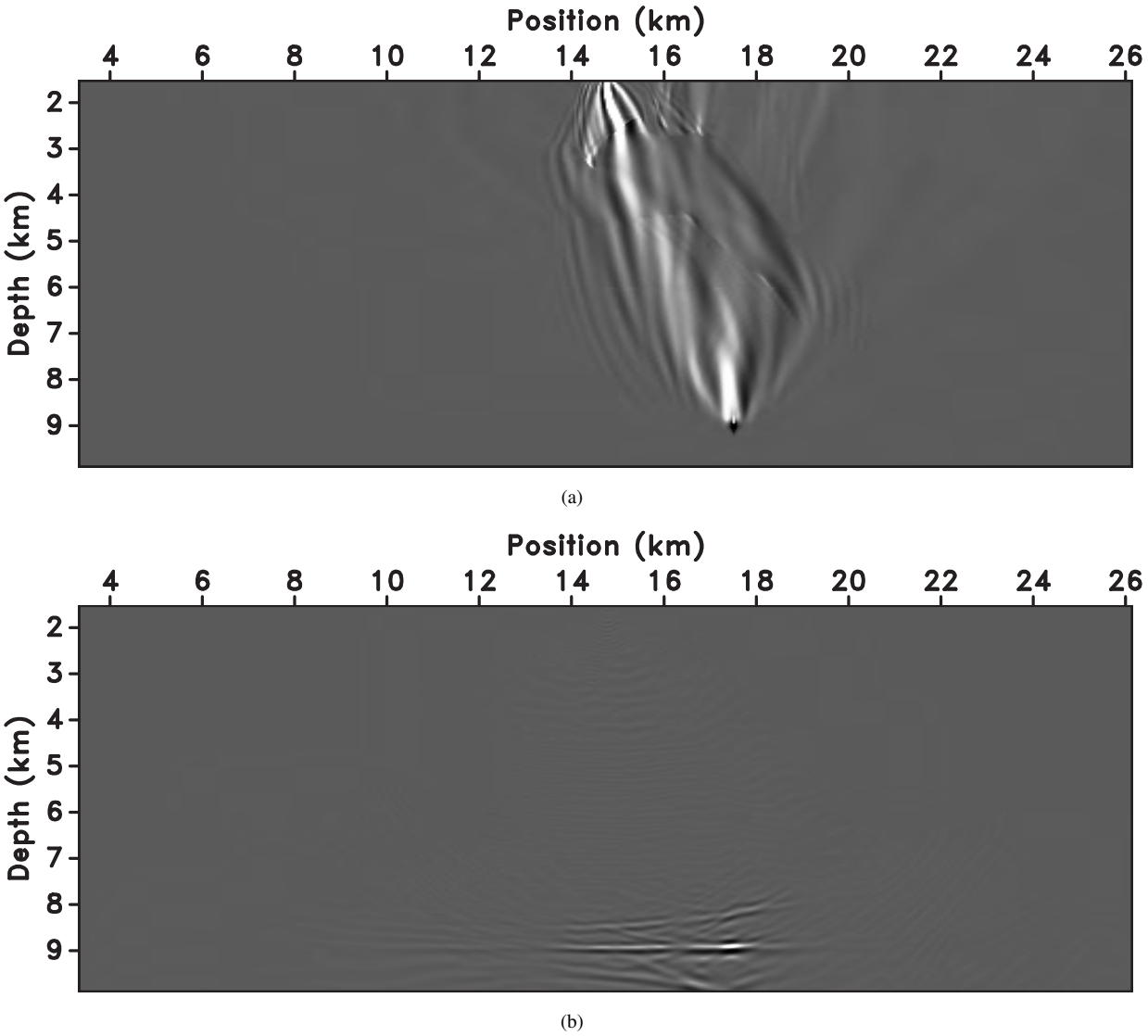

Figure 15. (a) Shot-record slowness perturbation obtained by the application of the adjoint scattering operator to the image perturbation from Figure 10(a) and (b) shot-record image perturbation obtained by the application of the forward scattering operator to the slowness perturbation from panel (a).

$u(\mathbf{m}) \xleftarrow{2D} u(\mathbf{k_m})$
$u(\mathbf{m}) * = e^{\pm i {k_z}^{\mathbf{x}} \Delta z}$

In this chart, ${k_z}^{\mathbf{k}}$ denotes the $\omega - \mathbf{k}$ component of the depth wavenumber and ${k_z}^{\mathbf{x}}$ denotes the $\omega - \mathbf{x}$ component of the depth wavenumber. An example of mixed-domain implementation is the Split-Step Fourier (SSF) method, where ${k_z}^{\mathbf{k}}$ represents the SSR equation computed with a constant reference slowness $\tilde{s}$, and ${k_z}^{\mathbf{x}} = \omega(s - \tilde{s})$ represents a space-domain correction (Stoffa *et al.*, 1990).

Based on the equation 28, the derivative of the depth wavenumber relative to slowness is

$$\left.\frac{dk_z}{ds}\right|_{s_0} = \frac{\omega}{\sqrt{1 - \left[\frac{|\mathbf{k_m}|}{\omega s_0(\mathbf{m})}\right]^2}} \,. \qquad \text{(A-1)}$$

The numeric implementation of the pseudo-differential equation A-1 is as complicated in media with lateral slowness variation as its phase-shift counterpart (equation 2). However, we can construct efficient and robust numeric implementations using similar approximations as the ones employed for the phase-shift relation, e.g. mixed-domain numeric implementation.

The linearized scattering operator can also be implemented in a mixed-domain by expanding the square-root from

relation A-1 using a Taylor series expansion

$$\left.\frac{dk_z}{ds}\right|_{s_0} \approx \omega \left(1+\sum_{j=1}^{N} c_j \left[\frac{|\mathbf{k_m}|}{\omega s_0\left(\mathbf{m}\right)}\right]^{2j}\right) , \qquad \text{(A-2)}$$

where c_j are binomial coefficients of the Taylor series.

Therefore, the wavefield perturbation at depth z caused by a slowness perturbation at depth z under the influence of the background wavefield at the same depth z (forward scattering operator 9) can be written as

$$\Delta u \approx \pm i\omega\Delta z \left(1+\sum_{j=1}^{N} c_j \left[\frac{|\mathbf{k_m}|}{\omega s_0}\right]^{2j}\right) u\Delta s \; . \qquad \text{(A-3)}$$

Similarly, the slowness perturbation at depth z caused by a wavefield perturbation at depth z under the influence of the background wavefield at the same depth z (adjoint scattering operator 12) can be written as

$$\Delta s \approx \mp i\omega\Delta z \left(1+\sum_{j=1}^{N} c_j \left[\frac{|\mathbf{k_m}|}{\omega s_0}\right]^{2j}\right) \overline{u}\Delta u \; . \qquad \text{(A-4)}$$

The mixed-domain implementation of the forward and adjoint scattering operators A-3 and A-4, is summarized on the following tables:

MIXED-DOMAIN IMPLEMENTATION OF THE FORWARD SCATTERING OPERATOR $\mathcal{F}^{\pm}_{ZOM}$ []

$\Delta w\left(\mathbf{m}\right) = \Delta s\left(\mathbf{m}\right) u\left(\mathbf{m}\right)$
$\Delta p\left(\mathbf{m}\right) = \Delta w\left(\mathbf{m}\right)$
$\Delta p\left(\mathbf{m}\right) \xrightarrow{2D} \Delta p\left(\mathbf{k_m}\right)$
$j = 1 \ldots N$ {
  $\Delta q\left(\mathbf{k_m}\right) = \Delta p\left(\mathbf{k_m}\right)$
  $\Delta q\left(\mathbf{k_m}\right) *= |\mathbf{k_m}|^{2j}$
  $\Delta q\left(\mathbf{m}\right) \xleftarrow{2D} \Delta q\left(\mathbf{k_m}\right)$
  $\Delta q\left(\mathbf{m}\right) *= \frac{c_j}{[\omega s_0(\mathbf{m})]^{2j}}$
  $\Delta w\left(\mathbf{m}\right) += \Delta q\left(\mathbf{m}\right)$
}
$\Delta w\left(\mathbf{m}\right) *= \pm i\omega\Delta z$

MIXED-DOMAIN IMPLEMENTATION OF THE ADJOINT SCATTERING OPERATOR $\mathcal{A}^{\mp}_{ZOM}$ []

$\Delta s\left(\mathbf{m}\right) = \Delta w\left(\mathbf{m}\right) \overline{u\left(\mathbf{m}\right)}$
$\Delta p\left(\mathbf{m}\right) = \Delta s\left(\mathbf{m}\right)$
$\Delta p\left(\mathbf{m}\right) \xrightarrow{2D} \Delta p\left(\mathbf{k_m}\right)$
$j = 1 \ldots N$ {
  $\Delta q\left(\mathbf{k_m}\right) = \Delta p\left(\mathbf{k_m}\right)$
  $\Delta q\left(\mathbf{k_m}\right) *= |\mathbf{k_m}|^{2j}$
  $\Delta q\left(\mathbf{m}\right) \xleftarrow{2D} \Delta q\left(\mathbf{k_m}\right)$
  $\Delta q\left(\mathbf{m}\right) *= \frac{c_j}{[\omega s_0(\mathbf{m})]^{2j}}$
  $\Delta s\left(\mathbf{m}\right) += \Delta q\left(\mathbf{m}\right)$
}
$\Delta s\left(\mathbf{m}\right) *= \mp i\omega\Delta z$

---

7 APPENDIX B: SUMMARY OF OPERATORS

All wave-equation migration velocity analysis operators described in the preceding sections are similar in that they relate perturbations of the image with perturbations of the (slowness) model. In all cases, this velocity estimation procedure takes advantage of features of migrated images which indicate incorrect imaging. The imaging inaccuracies can have several causes, i.e. incorrect downward continuation, irregular illumination, limited acquisition aperture etc., but the wave-equation MVA operators translate all inaccuracies in model updates. This feature, however, is a fundamental limitation of all migration velocity analysis techniques and we do not expand on this topic further.

Since the migration velocity analysis operators link image perturbations with slowness perturbations, they are all composed of several common parts, but with implementations that are specific for each imaging configuration. Thus, a wave-equation MVA operator is composed of an extrapolation operator (for wavefield reconstruction from recorded data), an imaging operator (for image construction from reconstructed wavefields) and a scattering operator (for relating wavefield perturbations to slowness perturbations). The following table summarizes the wave-equation MVA operator components in different imaging configurations, as described in detail in the preceding sections.

	extrapolation operator			**imaging operator**	**scattering operator**
	equation	velocity	time extrapolation	type	equation
zero-offset	SSR	half	backward	zero time	linearized SSR
	equations 1, 2			*equation 3*	*equations 9, 12*
survey-sinking	DSR	full	backward	zero time implicit cross-correlation	linearized DSR
	equations 13, 16			*equation 17*	*equations 21, 24,25*
shot-record	SSR	full	forward (source) backward (receiver)	zero time explicit cross-correlation	linearized SSR
	equations 26,27,28			*equation 29*	*equations 32,33,37,38*